Journal Pre-proof

Anthropogenic heat variation during the COVID-19 pandemic control measures in four Chinese megacities

Qingyan Meng, Jiangkang Qian, Uwe Schlink, Linlin Zhang, Xinli Hu, Jianfeng Gao, Qiao Wang

Please cite this article as: Q. Meng, J. Qian, U. Schlink, et al., Anthropogenic heat variation during the COVID-19 pandemic control measures in four Chinese megacities, *Remote Sensing of Environment* (2023), https://doi.org/10.1016/j.rse.2023.113602

Anthropogenic heat variation during the COVID-19 pandemic control measures in four Chinese megacities

Qingyan Meng[a,b,c], Jiangkang Qian[a,b,*], Uwe Schlink[d], Linlin Zhang[a,b,c], Xinli Hu[a,b,c], Jianfeng Gao[a,b], Qiao Wang[e]

a. Aerospace Information Research Institute, Chinese Academy of Sciences, Beijing, 100094, China
b. University of Chinese Academy of Sciences, Beijing, 100049, China
c. Key Laboratory of Earth Observation of Hainan Province, Hainan Aerospace Information Research Institute, Sanya, 572029, China
d. Department of Urban and Environmental Sociology, Helmholtz Centre for Environmental Research-UFZ, Leipzig, D-04318, Germany
e. Faculty of Geographical Science, Beijing Normal University, Beijing 100875, China
*Corresponding author: Jiangkang Qian
E-mail addresses: qianjiangkang20@mails.ucas.ac.cn

Abstract

Anthropogenic heat (AH) is an important input for the urban thermal environment. While reduction in AH during the Coronavirus disease 2019 (COVID-19) pandemic may have weakened urban heat islands (UHI), quantitative assessments on this are lacking. Here, a new AH estimation method based on a remote sensing surface energy balance (RS-SEB) without hysteresis from heat storage was proposed to clarify the effects of COVID-19 control measures on AH. To weaken the impact of shadows, a simple and novel calibration method was developed to estimate the SEB in multiple regions and periods. To overcome the hysteresis of AH caused by heat storage, RS-SEB was combined with an inventory-based model and thermal stability analysis framework. The resulting AH was consistent with the latest global AH dataset and had a much higher spatial resolution, providing objective and refined features of human activities during the pandemic. Our study of four Chinese megacities (Wuhan, Shanghai, Beijing, and Guangzhou) indicated that COVID-19 control

measures severely restricted human activities and notably reduced AH. The reduction was up to 50% in Wuhan during the lockdown in February, 2020 and gradually decreased after the lockdown was eased in April, 2020, similar to that in Shanghai during the Level 1 pandemic response. In contrast, AH was less reduced in Guangzhou during the same period and increased in Beijing owing to extended central heating use in winter. AH decreased more in urban centers and the change in AH varied in terms of urban land use between cities and periods. Although UHI changes during the COVID-19 pandemic cannot be entirely attributed to AH changes, the considerable reduction in AH is an important feature accompanying the weakening of the UHI.

Key words: anthropogenic heat; COVID-19 control; surface energy balance; hysteresis from heat storage; urban thermal environment

1. Introduction

The coronavirus disease 2019 (COVID-19) caused by the severe acute respiratory syndrome coronavirus triggered a global public health disaster in late December 2019 (Li et al., 2020; Zhou et al., 2021). Approximately 529 million confirmed cases and more than 6,299,000 deaths were reported worldwide by June 6, 2022 (WHO, 2022). China was the first country hit by the virus and a strict lockdown was implemented on January 23, 2020 in Wuhan, where the pandemic first occurred, to curb the spread of the virus (Zhou et al., 2021). The Wuhan lockdown was the first in modern public health history in a megacity with a population of more than 10 million. China also raised the national public health response to the highest level of emergency, involving measures that suspended public transportation and

entertainment and restricted non-essential activities and production to minimize the movement and gathering of people (Tian et al., 2020; Wang et al., 2020; Wilder-Smith and Freedman, 2020). Such lockdown and control measures effectively prevented the spread of the virus and avoided further infections (Atalan, 2020; Tian et al., 2020). The COVID-19 pandemic forced most countries to implement similar national control measures as China from March 2020 (Bar et al., 2021; Pal et al., 2021; Toseru et al., 2020). Although the COVID-19 control measures caused a global economic recession (The World Bank, 2020), they also resulted in temporary improvements in regional ecology (Bauwens et al., 2020; Liu et al., 2022b).

Transportation and industrial activities were considerably reduced during the lockdown and subsequent control measures, with a decrease in greenhouse gases, air pollutants, and aerosols, thus improving city air quality (Xe et al., 2020; Muhammad et al., 2020). Wang and Su (2020) observed lower concentrations of air pollutants (NO_2, CO, SO_2, and $PM_{2.5}$) in China during this time, with this trend beginning in Wuhan and spreading across the country, being strongly associated with travel restrictions (Bao and Zhang, 2020). Similar improvements in air quality were observed in Europe, America, India, Korea, Japan, and Russia (Bar et al., 2021; Ju et al., 2021; Wang and Li, 2021). Decreased atmospheric pollution not only mitigates respiratory diseases (Nicola et al., 2020; Sannino et al., 2021) but also affects the urban surface and atmospheric radiation balance. Higher daytime surface temperatures were expected during the lockdown in some cities because of air quality optimization, which increases the incident solar radiation (Parida et al., 2021; Shepherd,

2022). Surprisingly, several studies indicated significant reductions in surface temperature and urban heat island (UHI) intensity in China (Liu et al., 2022b), Europe, the United States (Parida et al., 2021), Middle East (El Kenawy et al., 2021), and India (Nanda et al., 2021) during the pandemic controls. Most studies attributed the UHI weakening to anthropogenic heat (AH) reduction caused by limited human activities; however, this has not been confirmed through quantitative AH studies during the pandemic are lacking. Therefore, the intensity of AH and its spatial distribution changes are still unknown in this anomalous period (Pal et al., 2021; Shepherd, 2022). Changes in the urban thermal environment are complicated, and various potential influencing factors should be clarified to analyze this process (Liao et al., 2017; Meng et al., 2022; Zhou et al., 2014). The COVID-19 epidemic caused an unprecedented anomalous scenario for urban thermal environments and AH is key to interpreting the characteristics of UHI changes due to the pandemic control measures.

AH is a source term in the urban energy balance and plays a vital role in urban climates (Nie et al., 2014; Zhou et al., 2012). Direct measurement of AH is challenging, but various estimation methods have been proposed, including the inventory-based method, surface energy balance (SEB) method, and building energy simulation (Grimmond, 1992; Sailor, 2011). AH is defined differently by the various methods. The inventory-based method assumes that heat from energy consumption is instantaneously emitted into the atmosphere, ignoring the hysteresis in heat release (Kotthaus and Grimmond, 2012; Smith et al., 2009). In contrast, the SEB method assesses the AH transferred and absorbed through the building envelope and released into the atmosphere via turbulent heat fluxes, long-wave radiation, etc.

(Liu et al., 2022a). The AH of these two methods is similar on longer time scales but inconsistent on shorter, sub-daily scales (Offerle et al., 2005; Pigeon et al., 2007). The reason for these differences could be the large heat storage owing to the thermal inertia of building materials (Liu et al., 2022a; Oke et al., 1999). The net rate of change in heat storage (ΔS) reflects the net absorption or release of energy, hereinafter as heat storage. Its role in urban areas is more notable than that in rural areas because of the differences in thermal properties, which is also an important factor contributing to UHI (Lindberg et al., 2020; Ramamurthy and Bou-Zeid, 2017). The non-negligible changes in heat storage caused by AH within urban areas (Grimmond and Oke, 1999; Yu et al., 2021) results in a hysteresis between AH emissions and urban temperature changes, which is contained in the residuals of the SEB.

The remote-sensing surface energy balance (RS-SEB) model proposed by Kato and Yamaguchi (2005) for AH estimation is a classical method, but the urban center AH based on this method is generally lower than that of the inventory-based method (Wong et al., 2015; Yu et al., 2021; Zhou et al., 2012). A major reason for this underestimation is the hysteresis of heat storage, as mentioned previously. In addition, the decrease in land surface temperature and albedo owing to building shadow could contribute to the partial AH underestimation of RS-SEB (Yu et al., 2021). The AH estimated from the RS-SEB cannot directly reflect human activities and energy consumption in comparison with the inventory-based method (Allen et al., 2011; Dong et al., 2017), which has advanced considerably in recent years owing to machine learning and big data techniques (Liu et al., 2021b; Ming et al., 2022; Qian et al., 2022; Xu et al., 2021). However, during COVID-19 control measures, the inventory-based

method was limited by insufficient data and empirical reliance, while RS-SEB could reflect the surface energy composition more objectively based on remote sensing images and meteorological conditions. Thus RS-SEB is a universal method for obtaining high-resolution AH (Yu et al., 2021), but the influence of ΔS needs to be avoided to more intuitively reflect AH changes induced by human activity anomalies during the COVID-19 pandemic. A combination of different AH estimation methods could be a potential solution (Chow et al., 2014; Wang et al., 2022; Zheng and Weng, 2018). In addition, the reduction in air pollutants during the pandemic slightly enhanced the solar radiation reaching the surface, yet the UHI showed an anomalous decreasing trend in most areas. And from the perspective of the more sensitive AH during the COVID-19 lockdown, this anomalous scenario is an excellent opportunity to explore the impact of human activities on the urban thermal environment.

This study focused on the period of the COVID-19 pandemic to 1) develop a high-resolution AH estimation method applicable to scenarios of various human activities, 2) explore the spatiotemporal characteristics of AH during COVID-19 control measures, and 3) investigate the association between AH and UHI during the lockdown. This study was conducted in four Chinese megacities (Beijing, Shanghai, Wuhan, and Guangzhou) before and after the pandemic.
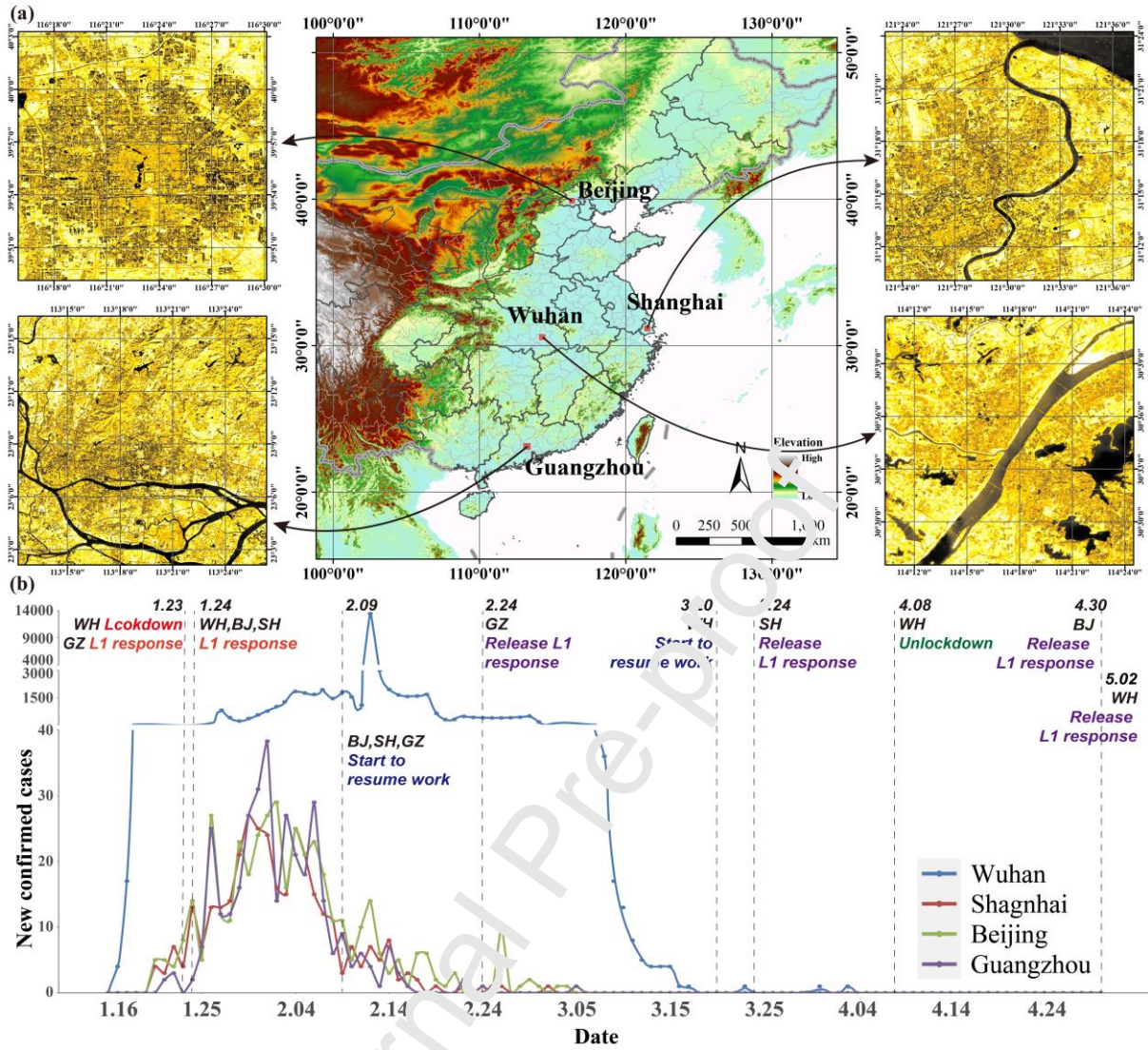
2. Study area and data set

2.1. Study areas

Wuhan, located in central China, is the capital of Hubei Province and has a population of over 12 million. As the first city to report COVID-19 cases, Wuhan adopted the strictest

lockdown measures on January 23, 2020 (Tian et al., 2020), involving the suspension of most socioeconomic activities and residential closures. After March 20, 2020, the city resumed work and production and the roadblocks that isolated Wuhan from the rest of the country were eased on April 8. Moreover, Beijing, Shanghai, and Guangzhou, three of China's most populous, largest, and powerful cities, also faced considerable impacts of the COVID-19 pandemic in early 2020. Therefore, lockdowns similar but relatively more lenient to that in Wuhan were adopted. Work and production gradually resumed around February 9 in most areas except Hubei Province, but a long term Level 1 response to public health emergencies was maintained (National Health Commission of the People's Republic of China, 2020). These four megacities are typical cases of AHI studies during the pandemic. Owing to limitations in RS image availability, only urban centers and cloud-free moments were used for this study (**Fig. 1a**).

The development of the pandemic in these four cities is illustrated in **Fig. 1b**. Note that to distinguish the different lockdown stages, "lockdown" in the following text only refers to the strictest control measures taken in Wuhan and Hubei Province at the beginning of the pandemic. The pandemic control measures of other cities or other periods will be called "L1 response".

Fig. 1. (a) Study area locations and albedo; (b) COVID-19 incidences in the four cities in early 2020 and important time points for pandemic control.

2.2. Data set

Landsat-8 Collection 2 Level 2 and Level 1 cloud-free data covering multiple temporal phases for the study area, Tokyo, and Seoul, for a total of 32 scenes (**Table A1**), were provided by the United States Geological Survey (https://earthexplorer.usgs.gov). Level 2 products included surface reflectance and surface temperature. For the not available part of Level 2 products, radiation calibration, atmospheric correction, and surface temperature retrieval were performed based on Level 1 products to obtain the corresponding data.

Landsat-8 data were used to calculate the SEB parameters and land cover classification. NASA digital elevation model (DEM) derived from the Shuttle Radar Topography Mission with a global 1 arc-second spacing (NASA JPL, 2020) was used to determine the surface altitude for calculating the relevant parameters. Finally, MOD11A1 daytime surface temperature data covering Wuhan were used to calculate the UHI intensity for the corresponding month, which was obtained from the LAADS website (https://ladsweb.nascom.nasa.gov).
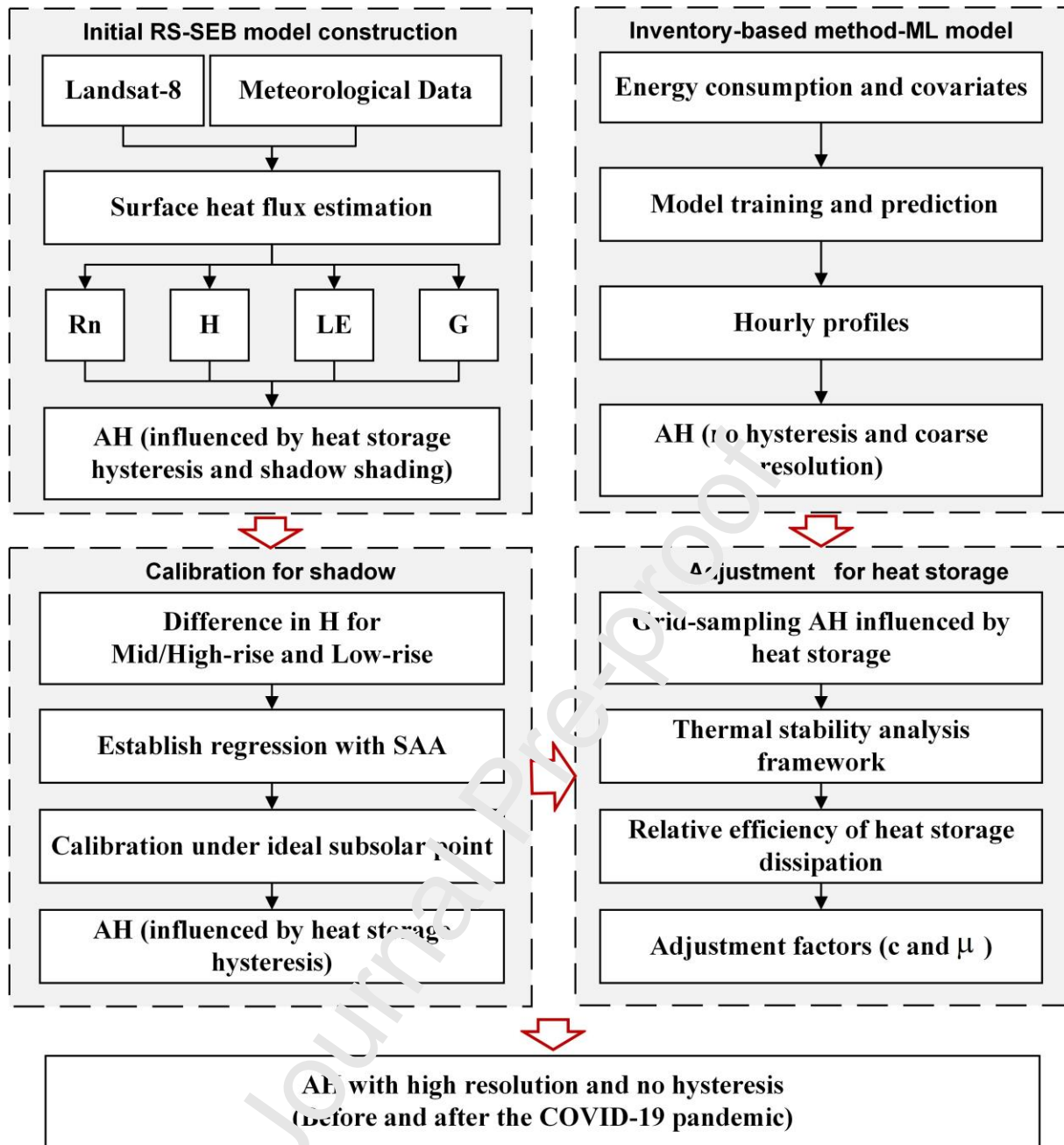
The meteorological data used for the SEB modeling included station observation data and the ERA5 hourly atmospheric reanalysis dataset corresponding to the time of satellite passing. Meteorological station data were hourly/sub-hourly observations from the National Centers for Environmental Information (NCEI CIG Team, 2021), including air temperature, wind speed, and dew-point temperature. ERA5 provides hourly space-continuous air temperature, wind speed, dew-point, and downwelling shortwave radiation at a spatial resolution of 31 km (Muñoz Sabater, 2019). The reanalysis data were corrected based on the average between the station data and reanalysis raster pixel values at the corresponding locations (Eq. (B.5)). Due to the absence of shortwave radiation observations, the reanalysis data were used directly, while relative humidity was estimated from air temperature and dew point.

Energy consumption, socio-economic statistics, points of interest, road networks, night-lights, normalized vegetation index, and other multi-source data were used to construct the machine learning model based on the energy inventory method in Section 3.1. The data source and pre-processing were based on a previous study (Qian et al., 2022) where the data

closest to the moment of satellite passing were selected. In addition, population heat maps representing the spatial aggregation of the population at different times of the day of the four cities were obtained based on the Baidu Huiyan big data platform (https://huiyan.baidu.com) for the hourly details of the inventory-based AH. The details and sources of the data used in the inventory-based method can be found in **Table A2**.

3. Methods

Here, we developed a new AH estimation method with high-resolution (see the workflow in **Fig. 2**) and four sections:1) inventory-based AH estimation combined with machine learning, 2) initial RS-SEB model construction, 3) shadow calibration of the initial RS-SEB model, and 4) adjustment of the ΔS impact on the estimated AH of RS-SEB. The inputs and outputs for each workflow in the study and some of the key abbreviations appearing are described in **Table 1**.

Fig. 2. Workflow of the study method. Rn: Net radiation; H: Sensible heat flux; LE: Latent heat flux; G: Ground heat flux; AH: Anthropogenic heat flux; SAA: Solar altitude angle; ML: Machine learning.

Table 1. Overall workflow information.

Workflow	Input	Key parameters	Output
Initial RS-SEB model	Meteorological data, multispectral remote sensing data	H: sensible heat flux. Rn: net radiation. G: Ground heat flux. LE: latent heat flux. $LULC$: land use and land cover.	AH_{SEB}
Inventory-based model	Multi-source data (**Table A2**)	f_{h-BT}: hourly factor of building and transportation heat. f_{h-I}: hourly factor of industrial heat.	AH_{Inv}
Calibration for shadow	AH_{SEB} (H, Rn, G, LE), LULC	R_{l-h}: the difference in H between low-rise and mid/high-rise buildings in percentage. R_{SS}^d: ideal percentage difference in the subsolar point assumption. SA_n: Solar altitude angle.	AH^{ns}
Adjustment for heat storage	AH_{Inv}, AH^{ns}, LULC	r_a, r_g: relative efficiency of energy dissipation by heat storage compared to sensible heat. c_i: adjustment factor of AH. μ_i: relative impact of ΔS on AH compared to H. $AH_{\Delta S}^{Grid}$: the ΔS perturbation caused by AH in the sampled grid.	AH

3.1. Inventory-based AH estimation

The inventory-based method assesses the heat directly generated by energy consumption without hysteresis from ΔS, which corresponds to the intensity of human activity within the city. Therefore, the results of this method can provide a reference for RS-SEB adjustments. The top-down inventory method is based on large-scale energy consumption, which is subsequently assigned to smaller spatiotemporal scales based on empirical laws (Allen et al., 2011; Flanner, 2009; Jin et al., 2019; Lu et al., 2017). We proposed a coarse-resolution (500 m) AH model combined with energy inventory and machine learning (Qian et al., 2022). The model was based on multi-source data and machine learning algorithms, which not only

improve the efficiency of AH estimation but provide a more refined representation of the spatiotemporal characteristics of AH from different sources (building, transportation, industrial heat). More information can be found in the original paper (Qian et al., 2022). Meanwhile, to obtain a more accurate AH close to the moment of satellite passing and avoid reconstructing the multiple years model, we replaced the original data of the model with data corresponding to the study temporal phase and supplemented the AH of Beijing based on the original modeling process. The hourly AH was derived from the hourly profile factors and the monthly AH results obtained from the model, as shown in Eq.(1) – (3):

$$AH_{Inv}^m = Model_E(Input)\#(1)$$

$$AH_{Inv}^h = f_{h-BT} \cdot AH_{BT}^m + f_{h-I} \cdot AH_I^m \#(2)$$

$$f_{h-BT} = \frac{POPheat_h}{1/24 \sum_0^{23} POPheat_h}\#(3)$$

where AH_{Inv}^m is the monthly multi-source AH derived from the model ($Model_E$) based on the energy inventory method and machine learning proposed in the previous study (Qian et al., 2022) and can be divided into monthly industrial heat AH_I^m and building and transportation heat AH_{BT}^m; AH_{Inv}^h is the hourly mean anthropogenic heat for the time corresponding to the passage of Landsat 8; f_{h-I} (%) is the hourly factor of industrial heat based on previous studies (Liu et al., 2021b; Zheng and Weng, 2018); f_{h-BT} (%) is the hourly factor estimated from the gridded hourly population heat value ($POPheat_h$), which depicts the distribution of people in the city in real-time based on the geographic location of cell phone users, which is one of the products of geographic big data and can effectively reflect the dynamic changes of the population (Lin et al., 2020). This study applied the hourly relative population heat values

for each grid to reflect the intra-day variation of human activity intensity (Eq. (3)), which provides a reasonable basis for the estimation of hourly profiles of building and transportation heat. AH_{Inv}^h is the hourly average value of the satellite crossing moment, which can express the instantaneous value of the AH at that moment given that AH does not vary much within one hour (Dong et al., 2017; Liu et al., 2021b). AH_{Inv}^h will be applied to the heat storage adjustment of the RS-SEB in Section 3.3.2.

3.2. Initial RS-SEB model

AH was initially estimated for four Chinese megacities based on the classical RS-SEB model (Kato and Yamaguchi, 2005; Kato and Yamaguchi, 2007; Zhou et al., 2012). The basic assumption of this method is that AH contributes only to the sensible heat flux; therefore, the results obtained by this method are the increases in sensible heat due to AH:

$$AH_{SEB} = H - (R_n - G - LE) = H - H_n \#(4)$$

where R_n is the net radiation, AH is the anthropogenic heat flux, H is the sensible heat flux, H_n is the sensible heat flux resulting from the radiative heat balance, and LE is the latent heat flux. In the case of no AH impact, the ground heat flux or conductive heat flux (G) is equivalent to the heat storage ΔS (Sun et al., 2017; Yu et al., 2021).

However, all other terms in the RS-SEB except sensible heat are also perturbed by AH but to a lesser extent (Kato and Yamaguchi, 2005), so the assumption of the RS-SEB model is not valid in reality but is still a relatively reasonable simplification in dry surface conditions. One of the most notable problems arising from this simplification is AH underestimation due to stronger ΔS in the urban center (Liu et al., 2022a; Yu et al., 2021; Zhou et al., 2012). The

SEB equation considering the ΔS perturbation is as follows:

$$R_n + AH = H + LE + (G + AH_{\Delta S}) \#(5)$$

where $AH_{\Delta S}$ is the perturbation of ΔS caused by anthropogenic heat, meaning the hysteresis between temperature change and heat emission. If $AH_{\Delta S}$ can be determined, then the value of AH can be calculated more accurately. However, currently, AH_{SEB} based on Eq. (4) cannot reflect the real heat generated by human activities owing to the hysteresis effect of ΔS, meaning that a part of the heat is stored during the day and released at night (Kato and Yamaguchi, 2007). Hysteresis can greatly interfere with the determination of AH during the COVID-19 pandemic, making it difficult to quantify variations in human activities under control measures. In addition, the overestimation of the temperature in shadowed areas may lead to an underestimation of H directly affecting the AH values and interfering with the adjustment of the ΔS impacts. Details of the initial RS-SEB modeling are shown in Appendix B.

3.3. AH adjustment of RS-SEB

3.3.1. Calibration for shadows

The surface temperature obtained from remote sensing is lower in shaded areas of medium/high-rise buildings (Kato and Yamaguchi, 2005), but coarse-resolution meteorological data cannot reflect air temperature decrease in shadowed areas, resulting in an underestimation of H in urban areas, eventually interfering with AH estimation. Here, a simple calibration procedure was established based on the idea that the building shadow interference decreases with an increasing solar altitude angle (SAA). The difference in the H

values between mid/high-rise and low-rise buildings at the image scale would change with the

SAA under the assumption of no shadowing in low-rise buildings. The relative percentage of

this difference (R_{l-h}) was calculated at the image scale, and an empirical relation was

established with the SAA at the corresponding moment of the remote sensing image:

$$H_{lr} = \delta_{S2}^{lr} H'_{lr} \#(6)$$

$$H_{hr} = \delta_{S1}^{hr} \delta_{S2}^{hr} H'_{hr} = \delta_{S1}^{hr} \beta \delta_{S2}^{lr} H'_{hr} \#(7)$$

$$R_{l-h} = \frac{H_{lr} - H_{hr}}{H_{lr}} = \frac{\left(H'_{lr} - \delta_{S1}^{hr} \beta H'_{hr}\right)}{H'_{lr}} \#(8)$$

where H_{lr} and H_{hr} are the mean values of sensible heat for low-rise and mid/high-rise

buildings in the image respectively; H' is the ideal sensible heat that is not perturbed by

shadows; δ_{S1}^{hr} are shadow perturbation terms (%) of H in mid/high-rise buildings; δ_{S2}^{lr} and

δ_{S2}^{hr} are ΔS perturbation terms (%) caused by AH in low-rise and mid/high-rise buildings,

respectively. $\beta = \delta_{S2}^{hr}/\delta_{S2}^{lr}$ is a constant value in this study (Appendix B), implying that the

δ_{S2}^{hr} characteristics were preserved without producing new perturbations when shadow

calibration was applied to mid/high-rise buildings. Furthermore, R_{l-h} can be expressed as a

function associated with the SAA:

$$R_{l-h} = 1 - (f_1(SAA) + \varepsilon_1) * \beta \frac{H'_{hr}}{H'_{lr}} = f_2(SAA) + \varepsilon_2 \#(9)$$
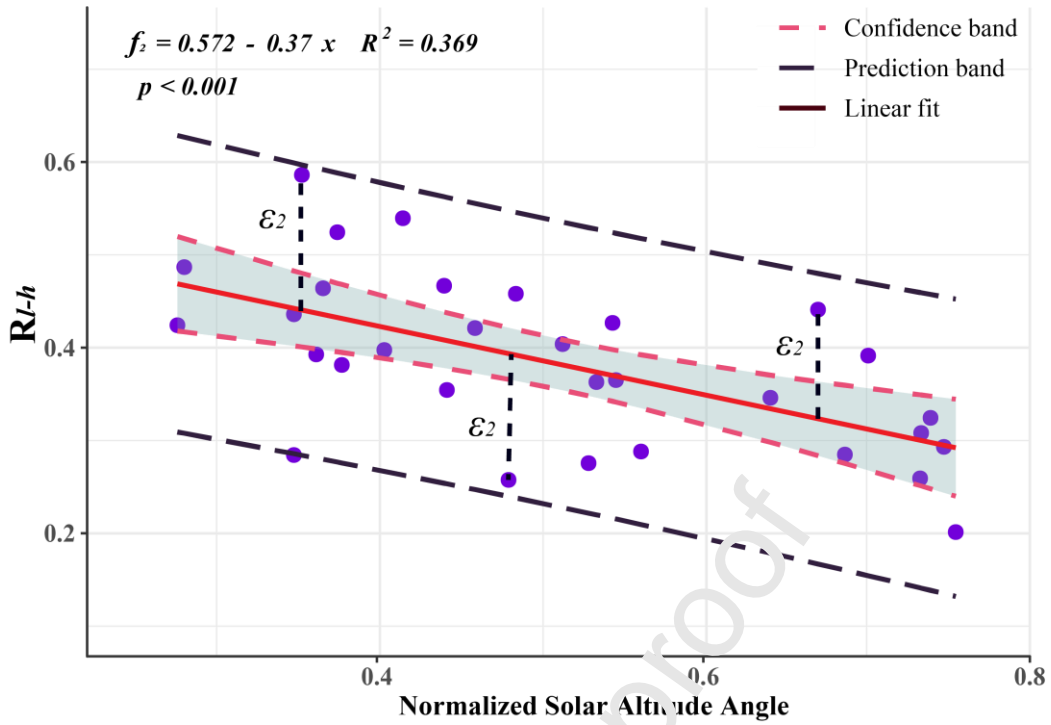
where ε is the error term and the final function $f_2(SAA)$ was fitted based on experiments

in different regions and periods (**Fig. 3**). Although the coefficient of determination R^2 was

approximately 0.37, there was a significant negative linear correlation between R_{l-h} and

SAA (p<0.001) for calibrating the H of mid/high-rise buildings.

$$R_{SS}^d = f_2(1) + \varepsilon_2^d \#(10)$$

$$H_{hr}^{ns} = \frac{1}{n} \sum\nolimits_{i=1}^{n} w_i (H_{lr}^i - H_{lr}^i R_{SS}^d) \#(11)$$

$$AH_{hr}^{ns} = (H_{hr}^{ns} + LE + G) - R_n \#(12)$$

Where R_{SS}^d is the ideal percentage difference of sample image d when the SAA (normalized) reaches a maximum of 1; ε_2^d is the error term unrelated to shadow impacts; H_{hr}^{ns} is the calibrated mid/high-rise building sensible heat on a pixel scale (if the calibrated value is lower than the pre-calibration value, the initial value is maintained, representing the unshaded image pixels); w_i is the inverse distance weight; n is the nearest low-rise pixel number of the mid/high-rise building pixels; and AH_{hr}^{ns} is the anthropogenic heat of mid/high-rise buildings after shadow calibration. The impact of shadow on H is a highly complex matter, which requires consideration of various factors, such as the building morphology, envelope structure, and shadow area separation, thus a more precise physical solution is a future focus to be addressed. At the same time, our method can be a more appropriate solution in case of insufficient experimental conditions. For instance, in the case of exploratory and comparative studies, such as the present study, which has less stringent requirements for absolute values, the great applicability of this method enables it to meet and support the AH studies with multiple scenarios.
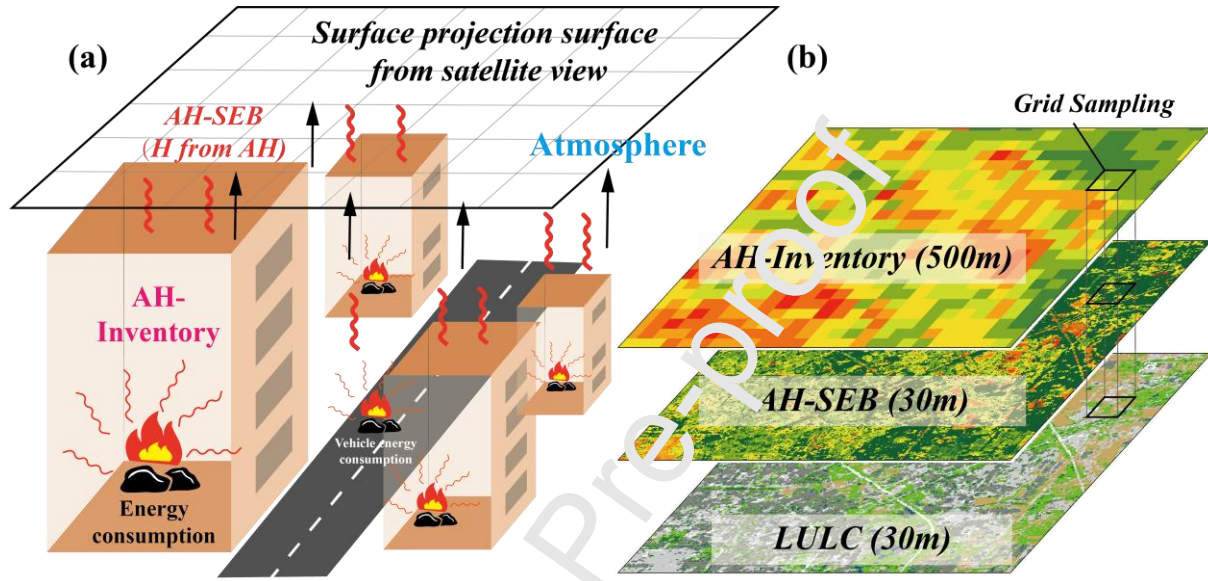
Fig. 3. Regression of sensible heat percentage difference between mid/high-rise and low-rise buildings with solar altitude angle.

3.3.2. *Adjustment for heat storage*

The heat generated by energy consumption with human activities (AH_{Inv}) is regarded as a common definition of AH because of the extensive applications of inventory-based methods, while the low AH_{SEB} in urban centers is considered an underestimation (Kato and Yamaguchi, 2005; Yu et al., 2021). However, not all the heat generated by human activities is instantaneously released into the atmosphere. In addition to the turbulent sensible heat exchange, expressed as the temperature change, AH may also be dissipated by long-wave radiation, latent heat, and heat storage (ΔS). In particular, ΔS has an important effect in urban built-up areas due to the thermal inertia of massive building materials (Grimmond and Oke, 1999; Roberts et al., 2006), the main reason for the hysteresis in AH conduction under the dry surface assumption, which leads to the difference between AH_{Inv} and AH_{SEB} (Liu et al.,

2022a; Yu et al., 2021). Thus, AH_{SEB} represents the increase in instantaneous sensible heat owing to AH, which is affected by the hysteresis of ΔS, while AH_{Inv} is the actual heat generated by human activities (**Fig. 4a**). The different representations of AH obtained by the two methods are reasonable in various scenarios.

Fig. 4. (a) Differences in anthropogenic heat (AH) estimated by the inventory-based method and remote sensing surface energy balance (RS-SEB); (b) Adjustment of AH from RS-SEB based on coarse resolution AH from the inventory-based method, LULC represents land use and land cover for r_a/r_g calculation.

In anomalous scenarios such as the COVID-19 pandemic lockdown or instances of war, the reliance on data and empirical laws reduces the applicability of inventory-based methods, and coupled with its coarse resolution, renders it unable to properly reflect anomalous AH features. Thus, we attempted to monitor AH changes during the pandemic using the RS-SEB model, which is more generalizable owing to lower data requirements. However, the hysteresis of AH release due to ΔS interferes with these results. We planned to determine the ΔS perturbations caused by anthropogenic heat ($AH_{\Delta S}$) in normal scenarios using the hysteresis-free AH_{Inv} as a reference (**Fig. 4b**). This was followed by an adjustment of the

AH_{SEB} (after shadow calibration) in combination with the relative efficiency of ΔS from the thermal stability analysis framework (Yu et al., 2021) and eventually extended to the anomalous scenario (**Fig. 5**). The thermal stability analysis framework based on the force-restore approach (Bateni and Entekhabi, 2012; Johnson et al., 1991) was used to quantify the relative efficiencies of the SEB components. Yu et al. (2021) proposed a stability analysis framework applied to AH perturbations to surface temperature:

$$\frac{d\delta T_s}{d\tau} = -\left(1 + \frac{r_a}{r_o} + \beta\frac{\delta_q}{\gamma} + \frac{r_a}{r_g}\right)\delta T_s + Q' \quad (13)$$

where δT_s is the surface temperature perturbation (K) caused by AH; τ is the nondimensional time scale; $\frac{r_a}{r_o}$, $\beta\frac{\delta_q}{\gamma}$, and $\frac{r_a}{r_g}$ represent the relative efficiency of energy dissipation by long-wave radiation, latent heat, and heat storage, respectively, compared to sensible heat; and Q' is the independent term of δT_s. Here, r_g represents the conductive heat resistance of the surface, depending on the thermal inertia of the material. More information on the framework and r_a/r_g calculations can be found in Appendix B. r_a/r_g can be understood simply as the ΔS efficiency but it is difficult to apply directly to urban areas where ΔS is stronger and more complicated. Here, AH_{SEB} was adjusted based on the relative values of r_a/r_g within the sampling grid corresponding to the AH_{Inv} as a reference. The adjustment scheme is illustrated as follows (**Fig. 5**):

$$AH_i = AH_i^{ns} + c_i[\overline{AH_{Inv}} - (\alpha_{HR}\overline{AH_{HR}^{ns}} + \alpha_{LR}\overline{AH_{LR}} + \alpha_R\overline{AH_R} + \alpha_I\overline{AH_I})]_{Grid}$$

$$= AH_i^{ns} + c_i AH_{\Delta S}^{Grid} \quad (14)$$

$$c_i = \left(\frac{r_a}{r_g}\right)_i / \sum_{j=1}^{n}\left(\frac{r_a}{r_g}\right)_j \frac{1}{n} \quad (15)$$

where AH_i is the adjusted anthropogenic heat of pixel i; AH_i^{ns} is the AH_{SEB} after shadow calibration; c_i is the adjustment factor of the corresponding pixel; $Grid$ is the sampling grid where pixel i is located; n is the number of pixels in the grid; $\overline{AH_{Inv}}$ is the mean anthropogenic heat of the inventory-based method in the grid; $\overline{AH_{HR}^{ns}}$, $\overline{AH_{LR}}$, $\overline{AH_R}$, and $\overline{AH_I}$ are mean AH_{SEB} for mid/high-rise (shadow-calibrated), low-rise, roads, and factories in the grid, respectively; α is the proportion (%) of the corresponding land cover types in the grid; and $AH_{\Delta S}^{Grid}$ represents the ΔS perturbation caused by AH in the sampled grid and the grid is not adjusted for $AH_{\Delta S}^{Grid}$ less than 0.
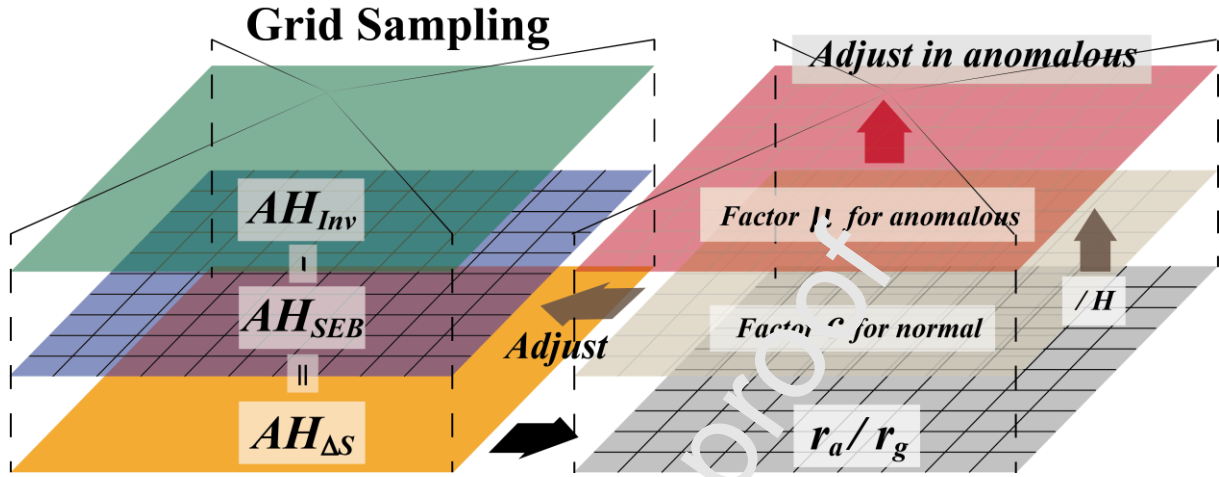
To avoid disturbance of the AH_{SEB}, the $AH_{\Delta S}^{Grid}$ and c_i calculated in normal scenarios were not directly used in the anomalous scenarios. Considering the similarity of land cover and meteorological conditions between the corresponding images of the two scenarios, and the insensitivity of the dissipation efficiency of ΔS relative to sensible heat to climate differences (Bateni and Entekhabi, 2012; Yu et al., 2021), we believe that the relative impact of ΔS obtained in normal scenarios is still valid in anomalous scenarios that violate the general distribution law of AH (Grimmond and Oke, 1999). Therefore, AH adjustment during COVID-19 control was calculated based on Eqs.(16) and (17):

$$AH_{i\_COVID} = AH_{i\_COVID}^{ns} + \mu_i H_{i\_COVID}^{ns} \#(16)$$

$$\mu_i = [\frac{c_i AH_{\Delta S}^{Grid}}{H_i^{ns}}]_{normal} \#(17)$$

where $AH_{i\_COVID}^{ns}$ is the shadow calibrated AH_{SEB} of pixel i during COVID-19 pandemic control and AH_{i_COVID} is the $AH_{i\_COVID}^{ns}$ after the heat storage adjustment; μ_i is the impact of ΔS relative to H for the normal months corresponding to the time of the pandemic

scenario; H_i^{ns} and $H_{i\_COVID}^{ns}$ are the sensible heat after shadow calibration in the same month during the normal scenario and COVID-19 pandemic control, respectively; and c_i is the adjustment factor for the normal scenario of the corresponding month.

Fig. 5. Schematic of AH_{SEB} (after shadow calibration) adjustment scheme in a sampling grid.

4. Results

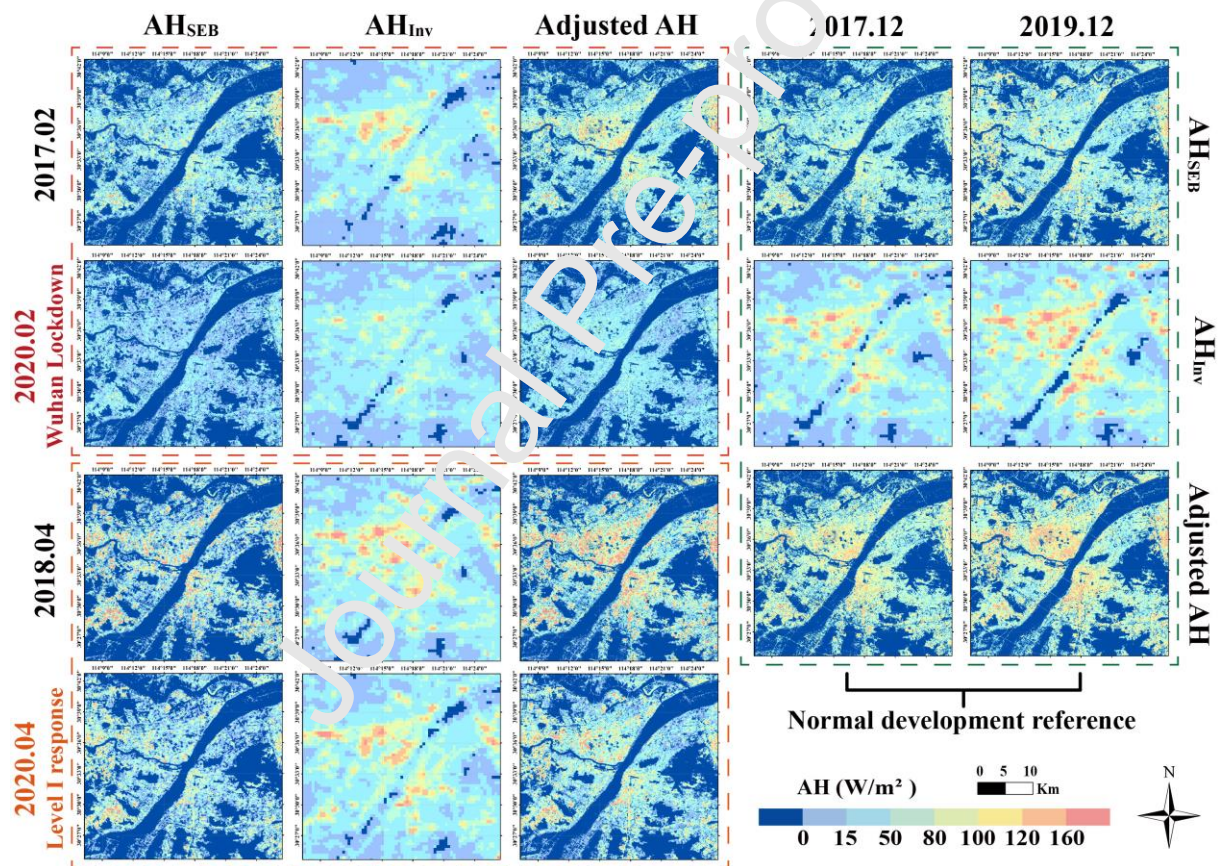### *4.1. AH of RS-SEB before and after adjustment*

AH_{SEB} and AH_{Inv} are similar in overall terms, but there are notable differences in spatial details. Similar to previous studies (Kato and Yamaguchi, 2005; Yu et al., 2021), the AH_{SEB} showed various magnitudes of underestimation in urban centers of several cities, and the spatial distribution characteristics were considerably different from those of AH_{Inv} (**Fig. A1 and A2**). We present a specific result of Wuhan as a case analysis (**Fig. 6**). AH_{Inv} shows more notable clustering characteristics than AH_{SEB}, with high values concentrated in the urban center and gradually decreasing in the suburban areas. The high values of AH_{SEB} were dispersed and notably lower than the values of AH_{Inv} in the urban center but the two methods were consistent in some suburban areas. The high intensity of energy consumption and strong heat storage in the urban center might contribute to the above differences, whereas

in other areas, although also affected by ΔS, the weaker intensity of human activities results in fewer AH differences. Thus, the adjustment for the ΔS impact was concentrated in central areas, whereas in some built-up areas far from the urban center, the AH_{SEB} tended to be larger than the AH_{Inv}, which was more evident in the northern industrial areas of Shanghai and Guangzhou. This phenomenon might be caused by higher G values in suburban areas owing to the fixed estimation factor (c_g) throughout the region (Oke et al., 2017; Yu et al., 2021). In addition, owing to the coarse spatial resolution of the inventory-based model, the pixels contained some small impervious surfaces, and AH_{Inv} exhibited heat emission in non-built-up areas. Regarding the comparison of different temporal phases, the RS-SEB model and inventory-based method were consistent in AH intensity across seasons. There were more areas with abnormally low AH_{SEB} values in spring than in winter, with more dramatic variations in the continuous space in spring. The stronger shadow impacts caused by higher temperatures and net radiation might be an important reason for the seasonal differences. Furthermore, AH_{SEB} and AH_{Inv} were consistent in the general characteristics of the annual variations, such as the AH growth in normal scenarios from 2017 to 2019 in Wuhan and Guangzhou. It is the association and differences between the two methods that contributed to the combined adjustment.

To ensure a reasonable representation of human activity intensity, the AH_{SEB} was greatly enhanced in the urban center after the adjustment, showing significant central aggregation characteristics like the AH_{Inv}, as well as retaining the temporal information of AH_{SEB} to help us explore the characteristics in anomalous scenarios. Its higher spatial resolution means

that it can express more detailed features. The AH of mid/high-rise buildings increased notably after the adjustment, as evidenced by the filling of the anomalous low AH_{SEB} voids in the city center, resulting in more diverse AH values within the city. More importantly, the adjusted RS-SEB is more comparable to other studies and represents AH without hysteresis corresponding to the intensity of human activity, rather than the increase in sensible heat flux due to AH, as defined by the initial model (Kato and Yamaguchi, 2005), which provides a more convenient condition for validation of the results.
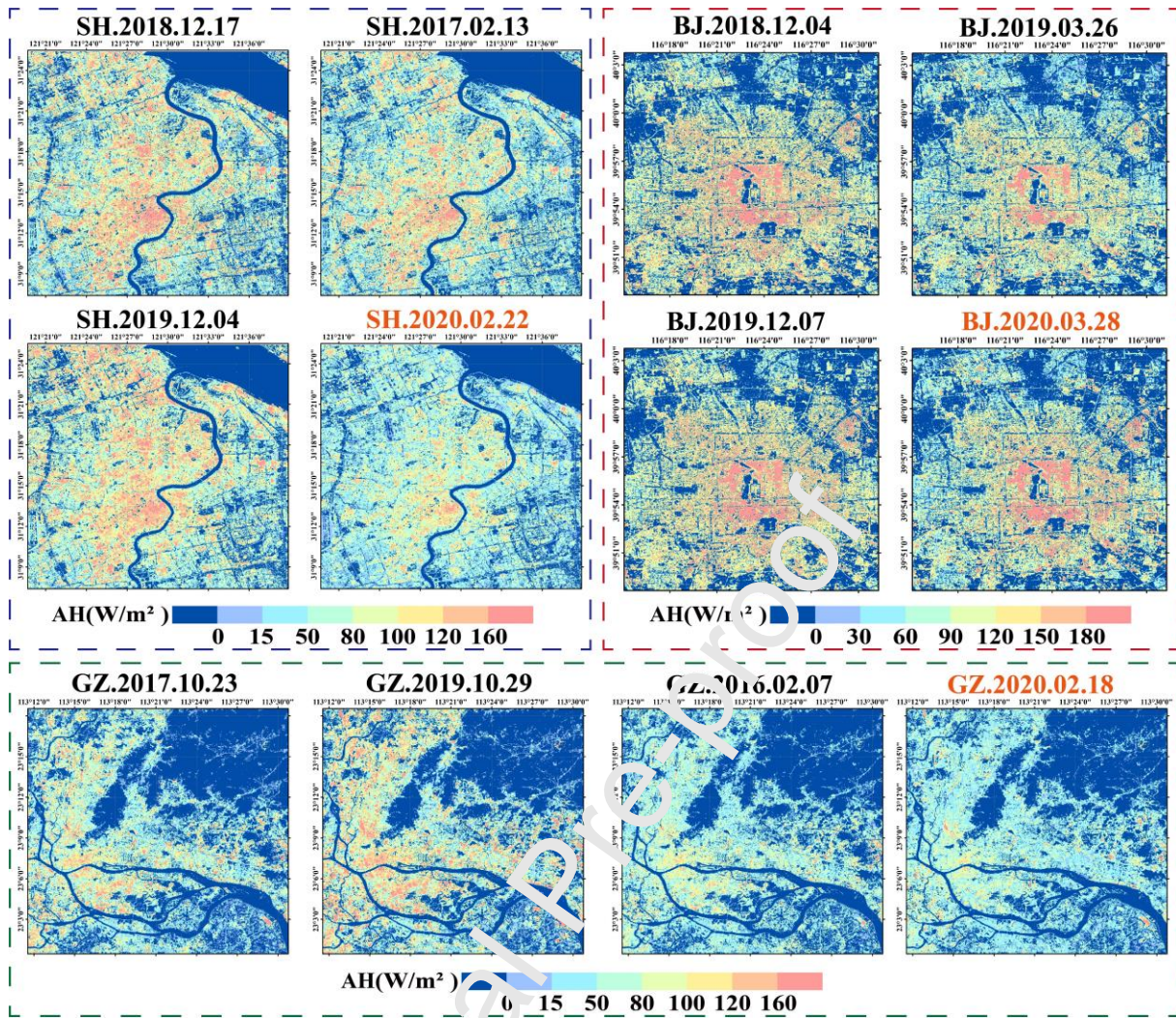

Fig. 6. Anthropogenic heat (AH) of different methods for different periods in Wuhan. The dates representing the Level 1 response and lockdown are highlighted in red, with different saturations.

4.2. AH variations during COVID-19 controls

China adopted rapid emergency response and control measures at the beginning of the

pandemic to control the spread of COVID-19. As the first and most seriously affected city of the pandemic, the AH in Wuhan was considerably reduced during the February, 2020 lockdown and did not completely recover after the lockdown was eased in April, 2020 (Zhou et al., 2021), but the results in December showed an increasing trend during normal scenarios (**Fig. 6**). This indicates that COVID-19 interrupted the healthy development trajectory of the city. A similar AH reduction occurred in Shanghai and Guangzhou during the L1 response in February, 2020 (**Fig. 7**), whereas the reduction was inconspicuous in Guangzhou. As an exception, the results of the adjusted AH in Beijing revealed an increase during the L1 response in March 2020, which is contrary to the results of the AH_{Inv} (**Fig. A1**). In general, from the AH maps, compared to the notable enhancement or weak variation in normal scenarios, cities except Beijing have different magnitude of reduction in AH especially in the urban centers under the pandemic control.
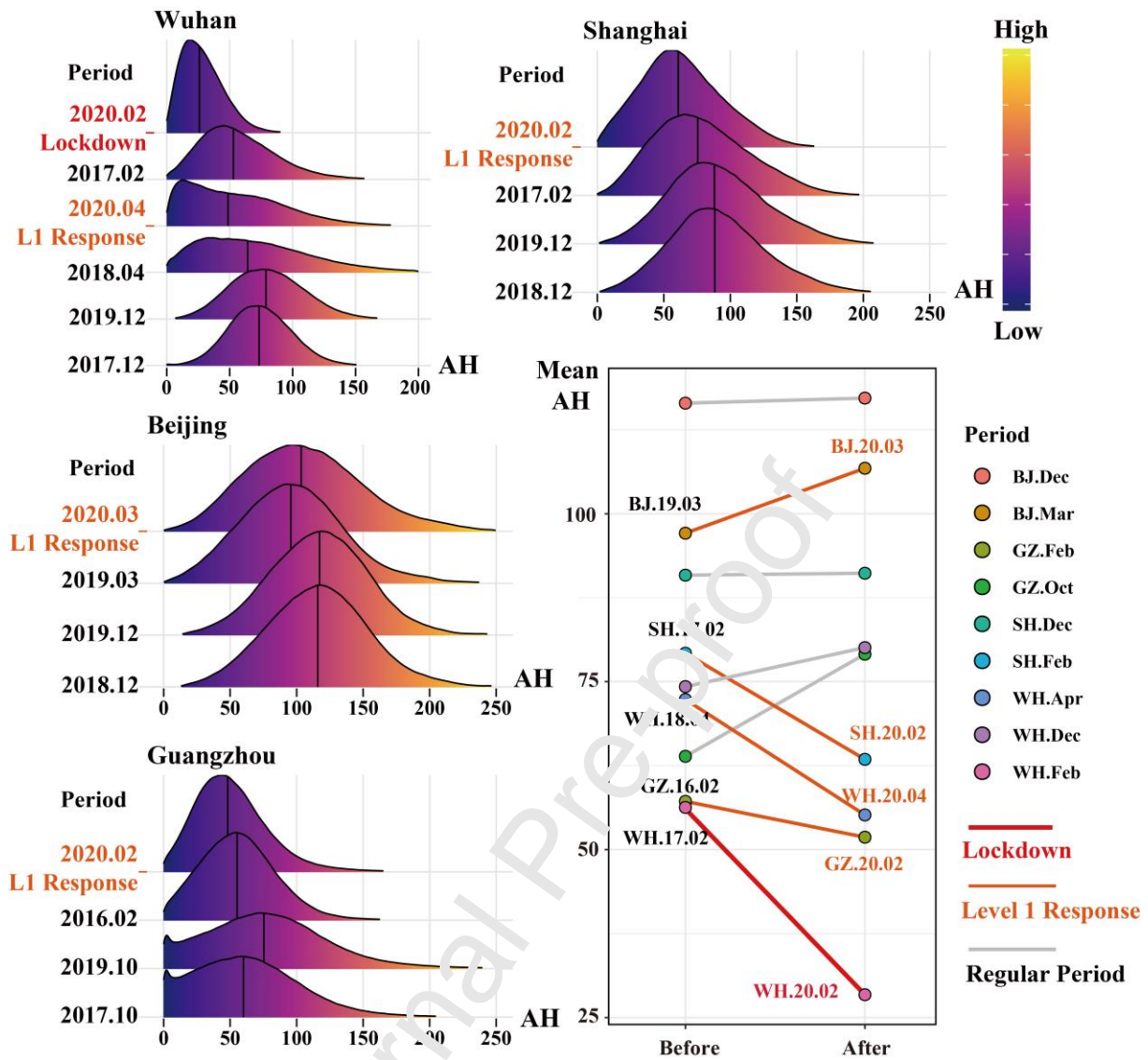
Fig. 7. Estimated Anthropogenic heat (AH) using the adjusted remote sensing surface energy balance (RS-SEB) model for Shanghai (SH), Beijing (BJ), and Guangzhou (GZ). The dates representing the Level 1 response are highlighted.

The numerical distribution mode of AH values for the same period between different years was similar under normal scenarios (**Fig. 8**). In winter, the AH numerical distribution was approximate to the normal distribution with a mean greater than 0 and a smaller standard deviation with relatively concentrated values, while in spring (Wuhan) and autumn (Guangzhou), the distribution of AH values was more dispersed. The AH of Beijing was considerably greater than that of other cities owing to the use of central heating, followed by Shanghai, which is comparable in urban scale to Beijing, while Guangzhou had the weakest

AH owing to a more comfortable climate in autumn and winter. In addition, AH increased in all four cities under normal scenarios but was weaker in Shanghai and Beijing. In contrast to the normal situation, during the COVID-19 control period, the distribution curve of AH values in all cities except Beijing moved leftward and the concentration of low values was more notable. These results reflect the general weakening of human activities throughout the urban area, which attenuated the spatial variability of AH values across the city. In particular, the largest AH reduction (average of 30 W/m^2) occurred during the Wuhan lockdown, while the reductions during the L1 response in Shanghai (16 W/m^2) and Wuhan (17 W/m^2) were similar but approximately half of that experienced in Wuhan under strict lockdown (**Fig. 8**). All the reductions were significant (p<0.001). This pattern is consistent with the intensity of control measures in restricting human activities.

Fig. 8. Numerical distribution of Anthropogenic heat (AH) in four cities at different stages and the slope of change over the same period in different years.

The spatial variation characteristics of AH resulting from COVID-19 control measures are shown at the block scale in Wuhan and Shanghai (**Fig. 9**), as the periods used for comparison in these two cities were typically less disturbed. Most areas of Wuhan exhibited significant reductions in AH during the lockdown, whereas in some areas around the urban center there was an increasing trend during the L1 response after the lockdown was eased. Furthermore, AH in the urban center increased as the reduction magnitude diminished as human activities recovered during the L1 response, presenting a trend of gradual recovery from suburban areas

to the center. A similar AH change characteristic appeared during the L1 response in Shanghai, but with a weaker reduction in the urban center, whereas the industrial areas in the north showed a more notable AH reduction. In combination with the essential urban land use categories (EULUC) (Gong et al., 2020), it is known that the mean AH reduction in the industrial and public service areas of Shanghai is 30%, while that in other areas is approximately 15% (**Fig. 9d** and **A3**). Further, residential areas had the smallest AH reduction due to the lower impact of pandemic control measures on human home activities, while industrial production, public facilities, and commercial activities were notably restricted and recovered more slowly than transportation facilities after the resumption of work. The AH of industrial areas in Wuhan was less affected (41%) compared to other EULUC during the lockdown, and the reduction of AH in other EULUC was approximately 50%, with the reduction of transportation and industrial facilities weakening to around 15% after the lockdown ended. However, human activities in commercial, residential, and public service areas were still greatly restricted (approximately 30% reduction), though there was a certain recovery. In summary, the restrictions on human activities during the Wuhan lockdown were much stronger than the ordinary control measures, and the AH reduction during the L1 response in Wuhan and Shanghai was similar at about 20%, but the AH change characteristics varied for land use categories.

Fig. 9. (a)-(c) Anthropogenic heat (AH) changes at block scale due to COVID-19 controls in February and April in Wuhan, and February in Shanghai; (d) AH reduction in terms of essential urban land use categories at different control stages; radar values represent relative magnitude of the AH reduction.

4.3. Relative and indirect validation

The results of the initial RS-SEB calculations were validated. The absolute values of SEB components are difficult to compare directly owing to the lack of measurement conditions and the variability of the experimental location and time, but the ratio of heat fluxes to net radiation can be used for relative validation to reflect model stability and reasonableness

(Kato and Yamaguchi, 2007; Weng et al., 2014). Comparing the RS-SEB of this study with previous estimations and practical observations in the literature, we confirmed our results for different seasons and cities (**Table A3**). Specifically, H/R_n was larger in summer than in winter and increased with the percentage of impervious surface, while LE/R_n also peaked in summer but decreased with the percentage of impervious surface, which could be attributed to summer high temperatures and greater evapotranspiration from the vegetation surface. The exception was the larger H/Rn in Beijing winters, which was also observed in Hu et al. (2012), which may be due to the centralized heating use and weaker net radiation in northern China winters. The RS-SEB we performed was in accordance with the criteria of previous studies.

The AH of the RS-SEB before and after adjustment were further validated using comparative validation based on correlation analysis, which is a common indirect validation method, due to the lack of actual AH measurement data (Firozjaei et al., 2020). The adjusted AH can be compared with recognized AH datasets, such as AH4GUC (Varquez et al., 2021) and PF-AHF (Jin et al., 2019), which are two recently proposed global AH datasets based on the idea of energy consumption but with a notably different construction process from the inventory-based method in this paper, which thus serve as good validation material. A significant ($p < 0.001$) correlation between the AH of RS-SEB and global AH datasets was found (**Table 2**), and the correlation of the adjusted results was markedly enhanced, indicating a stronger consistency between the adjusted AH and the common definition of AH at present. In addition, the adjusted AH had a more similar spatial distribution to the results of the model based on more refined data (Liu et al., 2021b; Sun et al., 2018), further demonstrating the

validity of the high-resolution AH estimation method proposed in this study, which can be

applied to AH monitoring during the COVID-19 pandemic.

Table 2. Correlation of the results of typical months in the general scenarios for this study before and after adjustment with the latest global AH dataset. Note that the AH4GUC contains hourly AH for each month in 2010, whereas the PF-AHF represents only the annual mean in 2015.

Area	Date	AH4GUC (2010)		PF-AHF (2015)	
		Initial	Adjusted	Initial	Adjusted
Wuhan	2017/02/16	0.49***	0.61***	0.23***	0.44***
	2017/12/17	0.45***	0.55***	0.3***	0.42***
	2018/04/08	0.44***	0.55***	0.28***	0.41***
Shanghai	2017/02/13	0.44***	0.54***	0.35***	0.56***
	2018/12/17	0.43***	0.54***	0.33***	0.54***
Beijing	2018/12/04	0.53***	0.72***	0.38***	0.52***
	2019/03/26	0.16**	0.7***	0.14***	0.52***
Guangzhou	2016/02/07	0.53***	0.6***	0.24***	0.5***
	2017/10/23	0.34***	0.58***	0.24***	0.49***

5. Discussion

5.1. Impacts of pandemic control on AH

The results demonstrate the considerable impact on urban human activities of the

COVID-19 pandemic and its control measures, which reduced AH while hindering normal

urban development, with the impact varying with the magnitude of the pandemic. The

lockdown in Wuhan, where the pandemic first started, halted most of the city's functions and

severely restricted people's movements. After the pandemic spread, Wuhan resumed

production activities and transportation to the outside world on April 8, 2020, while Shanghai

and Guangzhou, which experienced less impact from the pandemic, resumed work on

February 9 after a short period of strict control. Thus, although the cities still maintained the L1 response in the time we studied, the AH reduction was much lower than that during the strict lockdown measures. Although the results suggest a lower AH reduction in Guangzhou, it could be due to the effect of the comparison periods. Considering the rapid increase of AH in the last two years (October, 2017 to October, 2019) and that the Guangzhou image (February 2, 2016) used for comparison with the AH during the COVID-19 pandemic coincided with the Chinese New Year's Eve holiday, the AH reduction in Guangzhou during the L1 response could be much more than indicated by the current results. In contrast, AH changes in Beijing under pandemic control showed weakening and enhancement on AH_{Inv} and AH_{SEB}, respectively. Considering that the AH_{Inv} based on annual energy consumption and empirical patterns in general scenarios cannot accurately reflect the anomalous AH characteristics, the AH_{Inv} during the March 2020 pandemic may be unreliable. In addition, the original model of AH_{Inv} did not consider central heating energy consumption. Specifically, the causes of the AH increase in Beijing in March 2020 may be the longer central building heating time (lasting until March 31, 2020) because of COVID-19 control measures, while in 2019 the central heating lasted only until March 15. Therefore, the AH increases in this period based on RS-SEB could be more realistic. It also indicates that the RS-SEB may be more objective and applicable in anomalous scenarios.
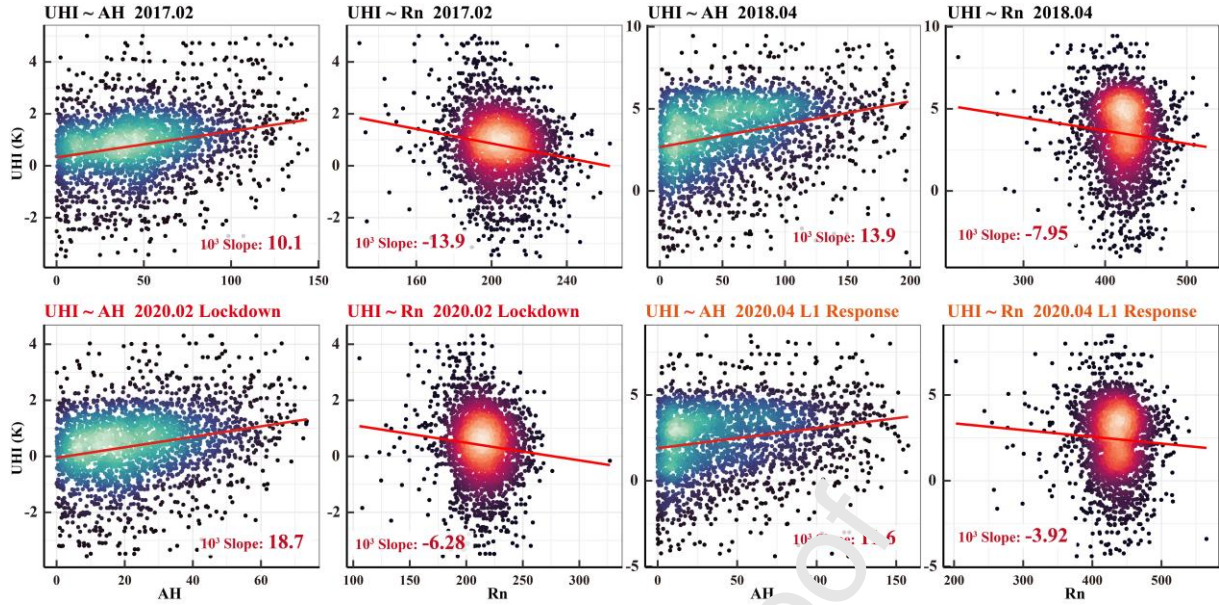
The spatial and temporal characteristics of AH during the COVID-19 pandemic reflect differences in human activity restrictions owing to different control measures and recovery strategies. For example, despite most traffic activities in Wuhan being stopped during the

lockdown, traffic facilities were also the fastest to resume after the lockdown was released for

the regular functioning of the city, while nonessential activities involving large human flows,

such as public services and commerce, resumed slowly. And such characteristics varied

among cities due to differences in policies and urban production requirements. Following the

resumption of urban human activities, energy consumption and AH may recover or even

exceed pre-pandemic levels (Wang and Su, 2020). Thus, the pandemic provides an excellent

opportunity to confirm whether AH reduction will optimize the urban thermal environment

and what spatiotemporal changes in AH are most beneficial, thus providing a theoretical basis

for subsequent urban planning and energy use studies.

5.2. *Relations between changes in UHI and AH*

Previously, due to the absence of AH data, it has been difficult to establish whether there

was a relationship between the decrease in UHI and reduction in AH during the COVID-19

control measures (Pal et al., 2021). This study provided some discussion of this issue and the

relationship between UHI (Liu et al., 2022b) and the two main energy inputs for the

corresponding months before and after the pandemic outbreak in Wuhan is shown in **Fig. 10**.

In general, AH had a marked promoting effect on UHI, while there was a simultaneous

negative correlation between R_n and UHI, with this negative correlation being stronger in

winter. Similar trends have been found in previous studies (Hou et al., 2022; Memon et al.,

2009) and because the R_n differences between urban and rural areas are small, this negative

correlation can be attributed to the difference in surface thermal properties. For example,

urban surfaces with low albedo receive more radiation, but a higher heat capacity or thermal

conductivity makes the temperature change insignificant, which is also an important factor determining a weaker UHI during daytime in winter. When shortwave radiation is enhanced to summer intensity, the relative impacts of heat storage can be weakened, implying a positive relationship change between radiation and temperature, enhancing daytime UHI (Zheng et al., 2021; Zhou et al., 2014), while the promotion effect of AH indicates its higher dissipation efficiency through sensible heat compared to R_n. During the lockdown, the lower AH had a steeper slope, implying that the UHI in this period was more sensitive to generally weakened AH and there was a greater spatial coherence between human activities and UHI intensity. However, the contribution of AH decreased slightly during the L1 response due to the spatial heterogeneity of the reduction or enhancement of AH within the city, thereby breaking the spatial coherence with the UHI (**Fig. 9**). It should be noted that such weak variations may also be natural fluctuations. The effect of R_n weakened during both the lockdown and L1 response, with the weakening closely related to the anomalous changes in AH or other factors because of the interactions among the UHI drivers (Hu et al., 2020). The driving mechanism of daytime UHI is complicated (Zhou et al., 2014); thus, there was no direct correlation between individual R_n and UHI but the positive effect of AH was notable.
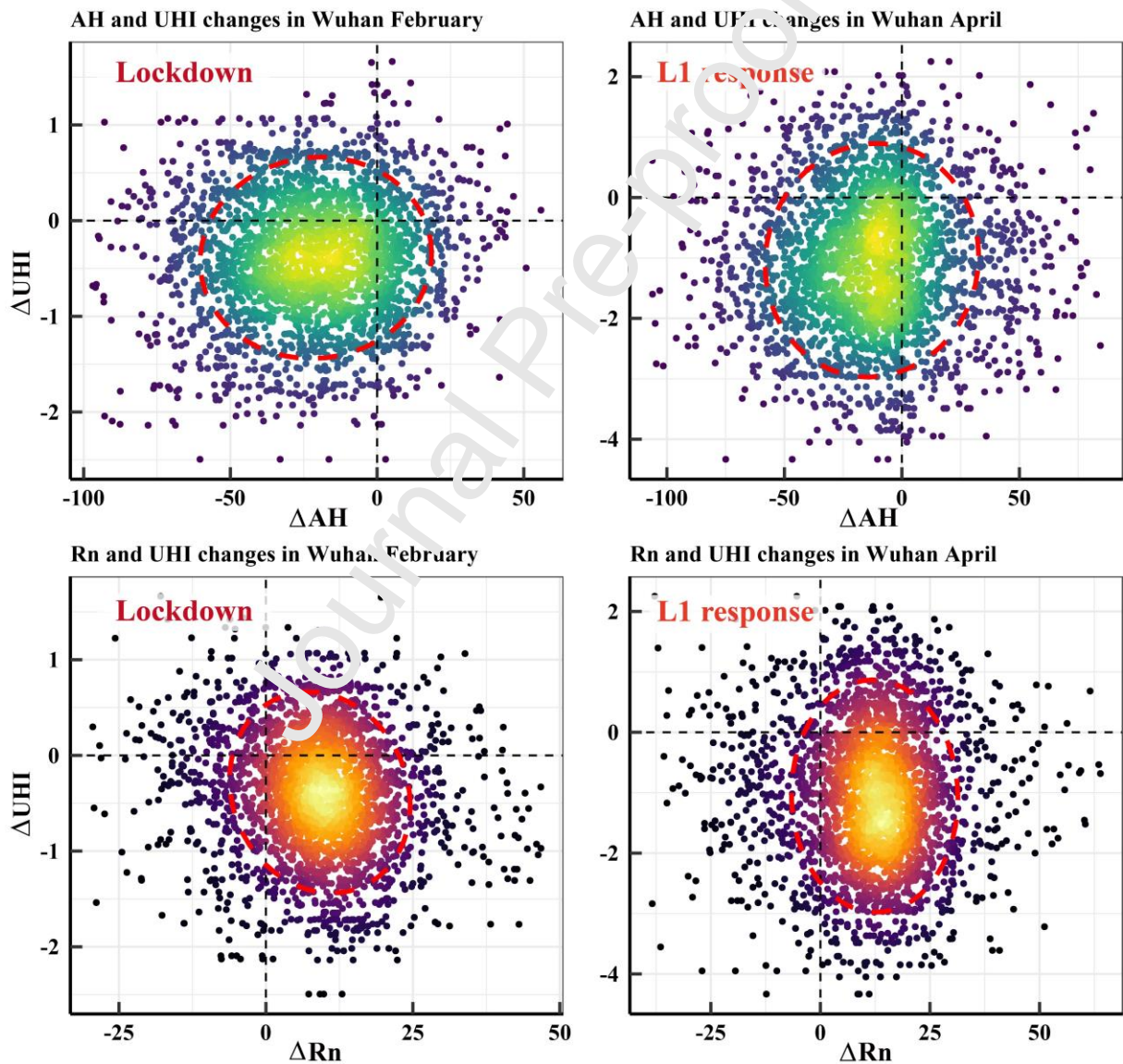
Fig. 10. Urban heat islands (UHI) scatter plot with AH and R_n in Wuhan for the corresponding months before and after the COVID-19 pandemic.

The changes in AH and R_n with the weakening of the UHI during the pandemic were discussed to examine the reasons for the abnormal change in UHI (**Fig. 11**). The trends of AH and R_n were almost exactly opposite but R_n was slightly enhanced; however, in the same region, a single R_n enhancement at different moments should not lead to UHI reduction. Thus, the current UHI anomaly is the result of a combination of multiple factors, with the marked reduction in AH, as another important urban energy input, being the most direct reason. Although the linear or monotonic relationship between ΔAH and ΔUHI was weak, most of the AH reduction corresponded to a decrease in the UHI. The magnitudes of AH and R_n variability during the L1 response were smaller and more concentrated compared to the lockdown, but the range of UHI variability was greater. In addition to the stronger daytime UHI baseline in spring (Hou et al., 2022), the complexity of this during the warm season indicates that other factors may also play a role, such as meteorological conditions, urban morphology, water distribution, and vegetation activity (Liu et al., 2021a; Wang et al., 2021;

Zhou et al., 2014). The anomalous changes in UHI during the pandemic cannot be fully explained at present but the significant reduction in AH is an important feature accompanying the weakening of the UHI, indicating the potential optimization of the urban thermal environment by controlling AH sources. Analysis of the UHI driving forces involving finer AH inputs as an important direction for future research will provide a more scientific, theoretical basis for urban planning and energy utilization.

Fig. 11. Anthropogenic heat (AH), R_n, and urban heat islands (UHI) changes in February (lockdown) and April (Level 1 response) in Wuhan compared to the periods before the pandemic. The red dashed ellipse contains 80% of the data.

5.3. Limitations and prospects

This study focused on the AH variations in four Chinese megacities during the COVID-19 pandemic in 2020, but uncertainties remained due to data availability limitations and the complexity of factors influencing AH. Limited by the coarse temporal resolution and cloud cover problems of Landsat, few images during the pandemic were available which led to uncertainties in the high-resolution AH results of this study. However, the climate conditions during the same months used for comparison differed little, thus its impacts might be small. Furthermore, the inventory-based model (Qian et al., 2022) in this study was established exactly on the impact factors of AH. In summary, based on the direct relationship between AH and human activities (Liu et al., 2022b; Shepherd 2022), it remains reasonable to attribute the AH changes during the pandemic to abnormal human activity restrictions, but a more detailed analysis of AH variability factors should be conducted in subsequent studies. The precise validation of AH is one of the key issues that need to be urgently addressed. Although the current AH estimation methods have been validated and developed based on local site flux observations (Chow et al., 2014; Pigeon et al., 2007), more convincing experiments for specific cases are required. However, due to the rigorous experimental conditions required for accurate flux field measurements (Sailor, 2011), most AH-related studies, both RS-SEB and inventory methods, use indirect validation (Firozjaei et al., 2020; Varquez et al., 2021). We believe that numerical meteorological simulations incorporating AH inputs could be an important tool for effective and convenient AH assessment in the future.

The spatial resolution of meteorological data should ideally match that of the remote

sensing data to achieve the highest accuracy and reliability of RS-SEB, but such data are hardly available due to the discontinuity and availability limitations of real meteorological stations. Therefore, this study followed the common assumption made in previous studies (Malbeteau et al., 2017; Weng et al., 2019; Yu et al., 2021) of using coarse-resolution data and station observations to represent meteorological conditions at the urban scale, which is based on the small variability and autocorrelation of general meteorological elements over a certain extension (Hubbard, 1994; Quinones et al., 2019). However, the neglect of spatial heterogeneity contributes to problems of scale mismatch. For example, the impacts of shadows on RS-SEB are caused by a mismatch between meteorological inputs and the high-resolution spatial details expressed by remote sensing (Kato and Yamaguchi, 2005; Yu et al., 2021). Although this study provided an approximate calibration for the shadow impacts, it is still challenging to fully clarify and resolve the issues associated with the scale mismatch. Apart from improvements in infrastructure and experimental equipment, this issue might be solved by data downscaling based on sophisticated numerical simulation models or deep learning algorithms, but effective examinations are lacking at present.

6. Conclusion

The reduction in urban AH due to COVID-19 controls might be an important reason for the decrease in UHI during this period and helps to clarify the AH variations during the pandemic for the interpretation and management of the urban thermal environment. To overcome the limitations of the initial RS-SEB model in AH representation owing to the impact of shadows and ΔS, this study proposed a high-resolution AH estimation method

without hysteresis by taking full advantage of the inventory-based method and RS-SEB model. The initial RS-SEB model had a notable underestimation of urban center AH compared to the results of the inventory-based method, which had a more dispersed distribution of high values and no obvious central aggregation characteristics. The results of the initial RS-SEB can be regarded as an increase in anthropogenic sensible heat influenced by ΔS, rather than AH in the general definition, and the effects of shadows cannot be ignored. The adjusted AH of RS-SEB was more correlated and consistent with the inventory-based AH datasets and had a much higher spatial resolution than the latter, which can thus represent more objective and finer human activities to apply to AH change monitoring during COVID-19 pandemic control measures.

AH estimation in four Chinese megacities showed that the COVID-19 pandemic and its control measures greatly reduced AH, providing practical evidence for optimizing the urban thermal environment through heat emission control measures. The AH in Wuhan was reduced by more than 50% during the strict lockdown in February, 2020 and gradually recovered after lockdown measures were relaxed in April, 2020. The AH reduction during the L1 response in Shanghai and Wuhan was similar, approximately half of that during the lockdown. Guangzhou had a smaller AH reduction in the same stage, while Beijing showed an increase in AH due to the extension of the centralized heating time. In addition, there was considerable spatiotemporal heterogeneity in AH changes during the COVID-19 pandemic, with urban centers tending to have greater reductions. Moreover, AH changes varied among the different land-use categories affected by the severity of pandemic control measures. The anomalous

changes in the UHI during the pandemic cannot be fully explained at present but the notable

reduction in AH is an important feature accompanying the weakening of the UHI. In addition,

multiple drivers of the urban thermal environment, such as canopy structure, climate, and

water distribution, should be further analyzed.

The AH adjustment method proposed in this study is empirically oriented, with

considerable potential for improvement. However, it promotes the integration of multiple

methods for AH estimation and establishes a foundation for meeting the AH requirements of

different scenarios. Furthermore, the exploration of AH and UHI in multiple scenarios will

provide diverse examples of evidence for subsequent studies and contribute to a deeper

understanding of the mechanisms driving the urban thermal environment to provide more

scientific solutions.

References

Allen, L., Lindberg, F., Grimmond, C.S.B., 2011. Global to city scale urban anthropogenic heat flux: model and variability. Int. J. Climatol. 31, 1990-2005

Atalan, A., 2020. Is the lockdown important to prevent the COVID-19 pandemic? Effects on psychology, environment and economy-perspective. Ann. Med. Surg. 56, 38-42

Bao, R., Zhang, A.C., 2020. Does lockdown reduce air pollution? Evidence from 44 cities in northern China. Sci.

Total Environ. 731, 139052

Bar, S., Parida, B.R., Mandal, S.P., Pandey, A.C., Kumar, N., Mishra, B., 2021. Impacts of partial to complete COVID-19 lockdown on NO2 and PM2.5 levels in major urban cities of Europe and USA. Cities 117, 103308

Bateni, S.M., Entekhabi, D., 2012. Relative efficiency of land surface energy balance components. Water Resour. Res. 48, W04510

Bauwens, M., Compernolle, S., Stavrakou, T., Muller, J.F., van Gent, J., Eskes, H., Levelt, P.F., van der A, R., Veefkind, J.P., Vlietinck, J., Yu, H., Zehner, C., 2020. Impact of Coronavirus Outbreak on NO(2)Pollution Assessed Using TROPOMI and OMI Observations. Geophys. Res. Lett. 47, e2020GL087978

Chow, W.T.L., Salamanca, F., Georgescu, M., Mahalov, A., Milne, J.M., Ruddell, B.L., 2014. A multi-method and multi-scale approach for estimating city-wide anthropogenic heat fluxes. Atmos. Environ. 99, 64-76

Dong, Y., Varquez, A.C.G., Kanda, M., 2017. Global anthropogenic heat flux database with high spatial resolution. Atmos. Environ. 150, 276-294

El Kenawy, A.M., Lopez-Moreno, J.I., McCabe, M.F., Dominguez-Castro, F., Pena-Angulo, D., Gaber, I.M., Alqasemi, A.S., Al Kindi, K.M., Al-Awadhi, T., Hereher, M.E., Robaa, S.M., Al Nasiri, N., Vicente-Serrano, S.M., 2021. The impact of COVID-19 lockdowns on surface urban heat island changes and air-quality improvements across 21 major cities in the Middle East. Environ. Pollut. 288, 117802

Firozjaei, M.K., Weng, Q.H., Zhao, C.H., Kiavarz, M., Lu, L.L., Alavipanah, S.K., 2020. Surface anthropogenic heat islands in six megacities: An assessment based on a triple-source surface energy balance model. Remote Sens. Environ. 242, 111751

Flanner, M.G., 2009. Integrating anthropogenic heat flux with global climate models. Geophys. Res. Lett. 36, L02801

Gong, P., Chen, B., Li, X.C., Liu, H., Wang, J., Bai, Y.Q., Chen, J.M., Chen, X., Fang, L., Feng, S.L., Feng, Y.J., Gong, Y.L., Gu, H., Huang, H.B., Huang, X.C., Jiao, H.Z., Kang, Y.D., Lei, G.B., Li, A.N., Li, X.T., Li, X., Li, Y.C., Li, Z.L., Li, Z.D., Liu, C., Liu, C.X., Liu, M.C., Liu, S.G., Mao, W.L., Miao, C.H., Ni, H., Pan, Q.S., Qi, S.H., Ren, Z.P., Shan, Z.R., Shen, S.Q., Shi, M.J., Song, Y.M., Su, M., Suen, H.P., Sun, B., Sun, F.D., Sun, J., Sun, L., Sun, W.Y., Tian, T., Tong, X.H., Tseng, Y.H., Tu, Y., Wang, H., Wang, L., Wang, X., Wang, Z.M., Wu, T.H., Xie, Y.W., Yang, J., Yang, J., Yuan, M., Yue, W.Z., Zeng, H.D., Zhang, K., Zhang, N., Zhang, T., Zhang, Y., Zhao, F., Zheng, Y.C., Zhou, Q.M., Clinton, N., Zhu, Z.L., Xu, B., 2020. Mapping essential urban land use categories in China (EULUC-China): preliminary results for 2018. Sci. Bull. 65, 182-187

Grimmond, C.S.B., 1992. THE SUBURBAN ENERGY-BALANCE - METHODOLOGICAL CONSIDERATIONS AND RESULTS FOR A MIDLATITUDE WEST-COAST CITY UNDER WINTER AND SPRING CONDITIONS. Int. J. Climatol. 12, 481-497

Grimmond, C.S.B., Oke, T.R., 1999. Heat storage in urban areas: Local-scale observations and evaluation of a simple model. J. Appl. Meteorol. 38, 922-940

He, G.J., Pan, Y.H., Tanaka, T., 2020. The short-term impacts of COVID-19 lockdown on urban air pollution in China. Nat. Sustain. 3, 1005–1011

Hou, H., Su, H., Liu, K., Li, X., Chen, S., Wang, W., Lin, J., 2022. Driving forces of UHI changes in China's major cities from the perspective of land surface energy balance. Sci. Total Environ. 829, 154710

Hu, D., Meng, Q., Zhang, L., Zhang, Y., 2020. Spatial quantitative analysis of the potential driving factors of

land surface temperature in different "Centers" of polycentric cities: A case study in Tianjin, China. Sci. Total Environ. 706, 135244

Hu, D., Yang, L., Zhou, J., Deng, L., 2012. Estimation of urban energy heat flux and anthropogenic heat discharge using aster image and meteorological data: case study in Beijing metropolitan area. J. Appl. Remote Sens. 6, 063559

Hubbard, K.G., 1994. SPATIAL VARIABILITY OF DAILY WEATHER VARIABLES IN THE HIGH-PLAINS OF THE USA. Agr. Forest Meteorol. 68, 29-41

Jin, K., Wang, F., Chen, D., Liu, H., Ding, W., Shi, S., 2019. A new global gridded anthropogenic heat flux dataset with high spatial resolution and long-term time series. Sci. Data 6, 139

Johnson, G.T., Oke, T.R., Lyons, T.J., Steyn, D.G., Watson, I.D., Voogt, J.A., 1991. SIMULATION OF SURFACE URBAN HEAT ISLANDS UNDER IDEAL CONDITIONS AT NIGHT .1. THEORY AND TESTS AGAINST FIELD DATA. Bound-Lay. Meteorol. 56, 275-294

Ju, M.J., Oh, J., Choi, Y.H., 2021. Changes in air pollution levels after COVID-19 outbreak in Korea. Sci. Total Environ. 750, 141521

Kato, S., Yamaguchi, Y., 2005. Analysis of urban heat-island effect using ASTER and ETM+ Data: Separation of anthropogenic heat discharge and natural heat radiation from sensible heat flux. Remote Sens. Environ. 99, 44-54

Kato, S., Yamaguchi, Y., 2007. Estimation of storage heat flux in an urban area using ASTER data. Remote Sens. Environ. 110, 1-17

Kotthaus, S., Grimmond, C.S.B., 2012. Identification of Micro-scale Anthropogenic CO2, heat and moisture sources - Processing eddy covariance fluxs for a dense urban environment. Atmos. Environ. 57, 301-316

Li, L., Li, Q., Huang, L., Wang, Q., Zhu, A., Xu, J., Liu, Z., Li, H., Shi, L., Li, R., Azari, M., Wang, Y., Zhang, X., Liu, Z., Zhu, Y., Zhang, K., Xue, S., Ooi, M.C.G., Zhang, D., Chan, A., 2020. Air quality changes during the COVID-19 lockdown over the Yangtze River Delta Region: An insight into the impact of human activity pattern changes on air pollution variation. Sci. Total Environ. 732, 139282

Liao, W.L., Liu, X.P., Wang, D.G., Sheng, Y.L., 2017. The Impact of Energy Consumption on the Surface Urban Heat Island in China's 32 Major Cities. Remote Sens. 9, 250

Lin, A., Wu, H., Liang, G., Cardenas-Tristan, A., Wu, X., Zhao, C., Li, D., 2020. A big data-driven dynamic estimation model of relief supplies demand in urban flood disaster. Int. J. Disast. Risk Re. 49, 101682

Lindberg, F., Olofson, K.F.G., Sun, T., Grimmond, C.S.B., Feigenwinter, C., 2020. Urban storage heat flux variability explored using satellite, meteorological and geodata. Theor. Appl. Climatol. 141, 271-284

Liu, W., Meng, Q., Allam, M., Zhang, L., Hu, D., Menenti, M., 2021a. Driving Factors of Land Surface Temperature in Urban Agglomerations: A Case Study in the Pearl River Delta, China. Remote Sens. 13, 2858

Liu, X., Yue, W.Z., Zhou, Y.Y., Liu, Y., Xiong, C.S., Li, Q., 2021b. Estimating multi-temporal anthropogenic heat flux based on the top-down method and temporal downscaling methods in Beijing, China. Resour. Conserv. Recycl. 172, 105682

Liu, Y., Luo, Z., Grimmond, S., 2022a. Revising the definition of anthropogenic heat flux from buildings: role of human activities and building storage heat flux. Atmos. Chem. Phys. 22, 4721-4735

Liu, Z.H., Lai, J.M., Zhan, W.F., Bechtel, B., Voogt, J., Quan, J.L., Hu, L.Q., Fu, P., Huang, F., Li, L., Guo, Z., Li, J.F., 2022b. Urban Heat Islands Significantly Reduced by COVID-19 Lockdown. Geophys. Res. Lett. 49, e2021GL096842

Lu, Y., Wang, H.K., Wang, Q.G., Zhang, Y.Y., Yu, Y.Y., Qian, Y., 2017. Global anthropogenic heat emissions from energy consumption, 1965-2100. Climatic Change 145, 459-468

Malbeteau, Y., Merlin, O., Gascoin, S., Gastellu, J.P., Mattar, C., Olivera-Guerra, L., Khabba, S., Jarlan, L., 2017. Normalizing land surface temperature data for elevation and illumination effects in mountainous areas: A case study using ASTER data over a steep-sided valley in Morocco. Remote Sens. Environ. 189, 25-39

Memon, R.A., Leung, D.Y.C., Liu, C.-H., 2009. An investigation of urban heat island intensity (UHII) as an indicator of urban heating. Atmos. Res. 94, 491-500

Meng, Q.Y., Hu, D., Zhang, Y., Chen, X., Zhang, L.L., Wang, Z.A., 2022. Do industrial parks generate intra-heat island effects in cities? New evidence, quantitative methods, and contributing factors from a spatiotemporal analysis of top steel plants in China. Environ. Pollut. 292, 118383

Ming, Y.J., Liu, Y., Liu, X., 2022. Spatial pattern of anthropogenic heat flux in monocentric and polycentric cities: The case of Chengdu and Chongqing. Sust. Cities Soc. 78, 103628

Muhammad, S., Long, X., Salman, M., 2020. COVID-19 pandemic and environmental pollution: A blessing in disguise? Sci. Total Environ. 728, 138820

[dataset] Muñoz Sabater, J., 2019. ERA5-Land hourly data from 1981 to present. https://doi.org/10.24381/cds.e2161bac

Nanda, D., Mishra, D.R., Swain, D., 2021. COVID-19 lockdowns induced land surface temperature variability in mega urban agglomerations in India. Environ. Sci-Proc. Imp. 23, 144-159

[dataset] NASA JPL, 2020. NASADEM Merged DEM Global 1 arc second. NASA EOSDIS Land Processes DAAC, V001. https://doi.org/10.5067/MEaSUREs/NASADEM/NASADEM_HGT.001

National Health Commission of the People's Republic of China, 2020. Epidemic control dynamics. http://www.nhc.gov.cn/xcs/yqfkdt/gzbd_index.shtml (accessed 30 May 2022)

[dataset] NCEI GIS Team, 2021. Hourly/Sub-Hourly Observational Data. V3.0.0. https://www.ncei.noaa.gov/maps/hourly/

Nicola, M., Alsafi, Z., Sohrabi, C., Kerwan, A., Al-Jabir, A., Iosifidis, C., Agha, M., Agha, R., 2020. The socio-economic implications of the coronavirus pandemic (COVID-19): A review. Int. J. Surg. 78, 185-193

Nie, W.-S., Sun, T., Ni, G.-H., 2014. Spatiotemporal characteristics of anthropogenic heat in an urban environment: A case study of Tsinghua Campus. Build. Environ. 82, 675-686

Offerle, B., Grimmond, C.S.B., Fortuniak, K., 2005. Heat storage and anthropogenic heat flux in relation to the energy balance of a central European city centre. Int. J. Climatol. 25, 1405-1419

Oke, T.R., Mills, G., Christen, A., Voogt, J.A., 2017. Urban climates. Cambridge University Press.

Oke, T.R., Spronken-Smith, R.A., Jauregui, E., Grimmond, C.S.B., 1999. The energy balance of central Mexico City during the dry season. Atmos. Environ. 33, 3919-3930

Pal, S., Das, P., Mandal, I., Sarda, R., Mahato, S., Nguyen, K.-A., Liou, Y.-A., Talukdar, S., Debanshi, S., Saha, T.K., 2021. Effects of lockdown due to COVID-19 outbreak on air quality and anthropogenic heat in an industrial belt of India. J. Clean Prod. 297, 126674

Parida, B.R., Bar, S., Kaskaoutis, D., Pandey, A.C., Polade, S.D., Goswami, S., 2021. Impact of COVID-19 induced lockdown on land surface temperature, aerosol, and urban heat in Europe and North America. Sust. Cities Soc. 75, 103336

Pigeon, G., Legain, D., Durand, P., Masson, V., 2007. Anthropogenic heat release in an old European agglomeration (Toulouse, France). Int. J. Climatol. 27, 1969-1981

Qian, J., Meng, Q., Zhang, L., Hu, D., Hu, X., Liu, W., 2022. Improved anthropogenic heat flux model for fine spatiotemporal information in Southeast China. Environ. Pollut. 299, 118917

Quinones, A.J.P., Cordoba, B.C., Gutierrez, M.R.S., Keller, M., Hoogenboom, G., 2019. Radius of influence of air temperature from automated weather stations installed in complex terrain. Theor. Appl. Climatol. 137, 1957-1973

Ramamurthy, P., Bou-Zeid, E., 2017. Heatwaves and urban heat islands: A comparative analysis of multiple cities. J. Geophys. Res.-Atmos. 122, 168-178

Roberts, S.M., Oke, T.R., Grimmond, C.S.B., Voogt, J.A., 2006. Comparison of four methods to estimate urban heat storage. J. Appl. Meteorol. Climatol. 45, 1766-1781

Sailor, D.J., 2011. A review of methods for estimating anthropogenic heat and moisture emissions in the urban environment. Int. J. Climatol. 31, 189-199

Sannino, A., D'Emilio, M., Castellano, P., Amoruso, S., Boselli, A., 2021. Analysis of Air Quality during the COVID-19 Pandemic Lockdown in Naples (Italy). Aerosol Air Qual. Res. 21, 200381

Shepherd, M., 2022. The Curious Relationship Between COVID-19 Lockdowns and Urban Heat Islands. Geophys. Res. Lett. 49, e2022GL098198

Smith, C., Lindley, S., Levermore, G., 2009. Estimating spatial and temporal patterns of urban anthropogenic heat fluxes for UK cities: the case of Manchester. Theor. Appl. Climatol. 98, 19-35

Sun, R., Wang, Y., Chen, L., 2018. A distributed model for quantifying temporal-spatial patterns of anthropogenic heat based on energy consumption. J. Clean Prod. 170, 601-609

Sun, T., Wang, Z.-H., Oechel, W.C., Grimmond, S., 2017. The Analytical Objective Hysteresis Model (AnOHM v1.0): methodology to determine bulk storage heat flux coefficients. Geosci. Model Dev. 10, 2875-2890

The World Bank, 2020. COVID-19 to Plunge Global Economy into Worst Recession since World War II. https://www.worldbank.org/en/news (accessed 30 May 2022)

Tian, H., Liu, Y., Li, Y., Wu, C.-H., Chen, B., Kraemer, M.U.G., Li, B., Cai, J., Xu, B., Yang, Q., Wang, B., Yang, P., Cui, Y., Song, Y., Zheng, P., Wang, Q., Bjornstad, O.N., Yang, R., Grenfell, B.T., Pybus, O.G., Dye, C., 2020. An investigation of transmission control measures during the first 50 days of the COVID-19 epidemic in China. Science 368, 638-642

Tosepu, R., Gunawan, J., Effendy, D.S., Ahmad, L.O.A.I., Lestari, H., Bahar, H., Asfian, P., 2020. Correlation between weather and Covid-19 pandemic in Jakarta, Indonesia. Sci. Total Environ. 725, 138436

Varquez, A.C.G., Kiyomoto, S., Khanh, D.N., Kanda, M., 2021. Global 1-km present and future hourly anthropogenic heat flux. Sci. Data 8, 1-14

Wang, K., Aktas, Y.D., Malki-Epshtein, L., Wu, D., Bin Abdullah, M.F.A., 2022. Mapping the city scale anthropogenic heat emissions from buildings in Kuala Lumpur through a top-down and a bottom-up approach. Sust. Cities Soc. 76, 103443

Wang, P., Chen, K., Zhu, S., Wang, P., Zhang, H., 2020. Severe air pollution events not avoided by reduced anthropogenic activities during COVID-19 outbreak. Resour. Conserv. Recycl. 158, 104814

Wang, Q., Li, S., 2021. Nonlinear impact of COVID-19 on pollutions - Evidence from Wuhan, New York, Milan, Madrid, Bandra, London, Tokyo and Mexico City. Sust. Cities Soc. 65, 102629

Wang, Q., Su, M., 2020. A preliminary assessment of the impact of COVID-19 on environment ? A case study of China. Sci. Total Environ. 728, 138915

Wang, Z., Meng, Q., Allam, M., Hu, D., Zhang, L., Menenti, M., 2021. Environmental and anthropogenic drivers of surface urban heat island intensity: A case-study in the Yangtze River Delta, China. Ecol. Indic. 128, 107845

Weng, Q., Firozjaei, M.K., Kiavarz, M., Alavipanah, S.K., Hamzeh, S., 2019. Normalizing land surface temperature for environmental parameters in mountainous and urban areas of a cold semi-arid climate. Sci. Total Environ. 650, 515-529

Weng, Q., Hu, X., Quattrochi, D.A., Liu, H., 2014. Assessing Intra-Urban Surface Energy Fluxes Using Remotely Sensed ASTER Imagery and Routine Meteorological Data: A Case Study in Indianapolis, USA. IEEE J. Sel. Top. Appl. Earth Obs. Remote Sens. 7, 4046-4057

WHO, 2022. WHO Coronavirus (COVID-19) Dashboard. https://covid19.who.int/info (accessed (30 May 2022))

Wilder-Smith, A., Freedman, D.O., 2020. Isolation, quarantine, social distancing and community containment: pivotal role for old-style public health measures in the novel coronavirus (2019-nCoV) outbreak. J. Travel. Med. 27, taaa020

Wong, M.S., Yang, J.X., Nichol, J., Weng, Q.H., Menenti, M., Chan, P.W., 2015. Modeling of Anthropogenic Heat Flux Using HJ-1B Chinese Small Satellite Image: A Study of Heterogeneous Urbanized Areas in Hong Kong. IEEE Geosci. Remote Sens. Lett. 12, 1466-1470

Xu, D., Zhou, D., Wang, Y.P., Meng, X.Z., Gu, Z.L., Yang, Y.J., 2021. Temporal and spatial heterogeneity research of urban anthropogenic heat emissions based on multi-source spatial big data fusion for Xi'an, China. Energy Build. 240, 110884

Yu, Z., Hu, L.Q., Sun, T., Albertson, J., Li, Q., 2021. Impact of heat storage on remote-sensing based quantification of anthropogenic heat in urban environments. Remote Sens. Environ. 262, 112520

Zheng, Y., Huang, L., Zhai, J., 2021. Divergent trends of urban thermal environmental characteristics in China. J. Clean Prod. 287, 125053

Zheng, Y., Weng, Q., 2018. High spatial- and temporal-resolution anthropogenic heat discharge estimation in Los Angeles County, California. J. Environ. Manage. 206, 1274-1286

Zhou, D.C., Zhao, S.Q., Liu, S.G., Zhang, L.X., Zhu, C., 2014. Surface urban heat island in China's 32 major cities: Spatial patterns and drivers. Remote Sens. Environ. 152, 51-61

Zhou, Y., Weng, Q., Gurney, K.R., Shuai, Y., Hu, X., 2012. Estimation of the relationship between remotely sensed anthropogenic heat discharge and building energy use. ISPRS-J. Photogramm. Remote Sens. 67, 65-72

Zhou, Y.n., Feng, L., Zhang, X., Wang, Y., Wang, S., Wu, T., 2021. Spatiotemporal patterns of the COVID-19 control measures impact on industrial production in Wuhan using time-series earth observation data. Sust. Cities Soc. 75, 103388

List of Figure Captions

Fig. 1. (a) Study area locations and albedo; (b) COVID-19 incidences in the four cities in early 2020 and important time points for pandemic control.

Fig. 2. Workflow of the study method. Rn: Net radiation; H: Sensible heat flux; LE: Latent heat flux; G: Ground heat flux; AH: Anthropogenic heat flux; SAA: Solar altitude angle; ML: Machine learning.

Fig. 3. Regression of sensible heat percentage difference between mid/high-rise and low-rise buildings with solar altitude angle.

Fig. 4. (a) Differences in anthropogenic heat (AH) estimated by the inventory-based method and remote sensing surface energy balance (RS-SEB); (b) Adjustment of AH from RS-SEB based on coarse resolution AH from the inventory-based method, LULC represents land use

and land cover for r_a/r_g calculation.

Fig. 5. Schematic of AH_{SEB} (after shadow calibration) adjustment scheme in a sampling grid.

Fig. 6. Anthropogenic heat (AH) of different methods for different periods in Wuhan. The dates representing the Level 1 response and lockdown are highlighted in red, with different saturations.

Fig. 7. Estimated Anthropogenic heat (AH) using the adjusted remote sensing surface energy balance (RS-SEB) model for Shanghai (SH), Beijing (BJ), and Guangzhou (GZ). The dates representing the Level 1 response are highlighted.

Fig. 8. Numerical distribution of Anthropogenic heat (AH) in four cities at different stages and the slope of change over the same period in different years.

Fig. 9. (a)-(c) Anthropogenic heat (AH) changes at block scale due to COVID-19 controls in February and April in Wuhan, and February in Shanghai; (d) AH reduction in terms of essential urban land use categories at different control stages. radar values represent relative magnitude of the AH reduction.

Fig. 10. Urban heat islands (UHI) scatter plot with AH and R_n in Wuhan for the corresponding months before and after the COVID-19 pandemic.
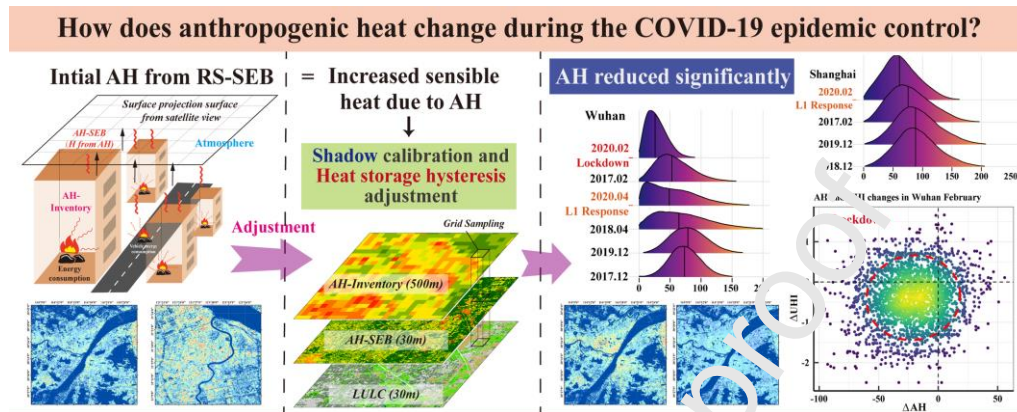
Fig. 11. Anthropogenic heat (AH), R_n, and urban heat islands (UHI) changes in February (lockdown) and April (Level 1 response) in Wuhan compared to the periods before the pandemic. The red dashed ellipse contains 80 % of the data.

Author Statement

Qingyan Meng: Supervision, Writing-Original Draft, Conceptualization, Investigation, Formal analysis, Funding acquisition. **Jiangkang Qian:** Project administration, Writing-Original Draft, Conceptualization, Methodology, Software. **Uwe Schlink:** Supervision, Writing-Reviewing and Editing, Conceptualization. **Linlin Zhang:** Project administration, Writing-Reviewing, Funding acquisition. **Xinli Hu:** Resources, Writing - Editing. **Jianfeng Gao:** Writing- Editing, Data curation **Qiao Wang:** Resources, Funding acquisition.

Declaration of interests

The authors declare that they have no known competing financial interests or personal

relationships that could have appeared to influence the work reported in this paper.

Highlights of the study

- A high-resolution anthropogenic heat estimation method for special scenarios
- A novel adjustment method was developed to estimate the surface energy balance
- Practical evidence was provided for optimizing the urban thermal environment
- COVID-19 pandemic and its control measures greatly reduced anthropogenic heat